TÜBİTAK

Turkish Journal of Earth Sciences

http://journals.tubitak.gov.tr/earth/

Research Article

Turkish J Earth Sci
(2020) 29: 221-241

doi:10.3906/yer-1905-20

Last glacial climate oscillations and sudden environmental changes investigated in stalagmites from southwest Sulawesi, western Pacific

Ezgi ÜNAL İMER[1,2,*], İbrahim Tonguç UYSAL[1,3], Emma ST PIERRE[4], Jian-Xin ZHAO[1], James SHULMEISTER[1]

[1]School of Earth & Environmental Sciences, University of Queensland, Brisbane, Australia
[2]Department of Geological Engineering, Faculty of Engineering, Middle East Technical University, Ankara, Turkey
[3]Commonwealth Scientific and Industrial Research Organisation (CSIRO), Energy, Kensington, Australia
[4]School of Social Science, University of Queensland, Brisbane, Australia

Received: 29.05.2019 • **Accepted/Published Online:** 02.10.2019 • **Final Version:** 15.01.2020

Abstract: We investigated two stalagmites from the Saripa Cave and Bumi Cave in southern Sulawesi, Indonesia, using high-precision U-series dating and high-resolution trace element and C-O-Sr isotope analysis. The growth record (from 10.4 ± 0.1 ka to 77.4 ± 0.9 ka) of the Saripa Cave stalagmite (SR04-ST3) is fragmented with two major (at the top: 10.4–11.6 ka and middle: 43.8–44.7 ka sections of the stalagmite) and some short (middle and bottom sections) growth phases, interrupted by long-lasting growth hiatuses. Both the timing of the growth phases and the $\delta^{18}O$ values for different growth phases are correlated with those of cold/dry (~22 ka and 43.8–44.7 ka) and wet/warm periods (e.g., Greenland Interstadials 12, 14, and 21) in the northern hemisphere speleothem records, displaying both anti-phase and in-phase relationships with the northern hemisphere records. This observation is unique in the Western Pacific tropical region, mostly likely because the Saripa Cave is located within the region of the latitudinally migrating Intertropical Convergence Zone (ITCZ), whereby the rainfall seasons may have changed through time depending on the mean latitude of the ITCZ. The Saripa Cave stalagmite contains textural laminae, which are here interpreted as a record of rapid environmental changes, possibly caused by volcanic eruptions at around 22.55 ka and 44.73 ka BP. The Bumi Cave record (stalagmite BC-09-3-C), on the other hand, presents very little variation in stable isotope and trace element compositions between 26.8 ka and 18.5 ka and does not seem to be influenced by any possible volcanic activity. More detailed future studies investigating millimeter- to submillimeter-scale geochemical time-series constrained by accurate ages in speleothems can be useful in unfolding the effects of eruptions and provide parallel records of climate and sudden environmental changes.

Key words: Stalagmite, U-series dating, isotope geochemistry, trace elements, past climate

1. Introduction

Cave carbonate mineral deposits, also known as speleothems, provide a unique opportunity to reconstruct climate changes, human evolution, recurrence patterns of paleoseismic events, and volcanic eruptions (e.g., Wang et al., 2001; Zhao et al., 2001; Fleitmann et al., 2004, 2009; Kagan et al., 2005; Tuccimei et al., 2006; Frisia et al., 2008; Wynn et al., 2008; Siklosy et al., 2009; Badertscher et al., 2014; Jamieson et al., 2015). While the importance of speleothems as archives of climate change has been well established, their role in the reconstruction of Earth's volcanism is still in its infancy. However, high-precision U-series dating and high-resolution geochemical analyses of speleothems have the potential to provide parallel records of climate and environmental change, and thus offer insights into the complex interplay of tectonics and hydroclimatological processes. It has been reported that oxygen and carbon isotope records in cave speleothems and travertine deposits show episodic CO_2 release events related to major episodes of volcanic activity (Tuccimei et al., 2006; D'Alessandro et al., 2007). Similarly, trace elements, together with stable and Sr isotope compositions of vein carbonate samples, are excellent indicators for the origin of CO_2-bearing fluids, providing essential information on the long-term evolution of geothermal systems in tectonically active regimes (Uysal et al., 2009, 2011; Ünal-İmer et al., 2016b). Furthermore, sulfate concentration peaks in speleothems from northern Turkey and the Italian Alps have been used successfully as archives of precisely dated past volcanism, coinciding with the Santorini eruption and the Tambora and Krakatau eruptions, respectively (Frisia et al., 2008 and references therein; Badertscher et al., 2014).

Indonesia is a particularly apt location to test the interplay of volcanism and hydroclimatological processes.

* Correspondence: eunal@metu.edu.tr

Its climate evolution is highly complex because of a number of uncertainties regarding the dynamics of the Indo-Pacific Warm Pool (IPWP) hydroclimate (Cane and Clement, 1999; Visser et al., 2003; Wurtzel et al., 2018), as well as the role of explosive volcanism in the region. Speleothem $\delta^{18}O$ records from Flores mainly document southern hemisphere (SH) climate signals and sea-level rise (Griffiths et al., 2009; Ayliffe et al., 2013), whereas the Borneo records indicate that the tropical Pacific hydrological cycle is responsive to high-latitude climate processes in both hemispheres (Partin et al., 2007). Climate proxies from Sulawesi represented by geochemical and isotopic records from leaf waxes (for the last 15,000 years, Tierney et al., 2012) and lake sediment cores that span the past 60,000 years (Russel et al., 2014) suggest that the hydrological variability in this part of Indonesia changes significantly in response to high-latitude climate forcing, as was also recorded in Borneo stalagmites (Partin et al., 2007). This is probably a result of reorganizations of the monsoons and the latitudinal position of the Intertropical Convergence Zone (ITCZ) (Russel et al., 2014). U-series dates of minicores extracted in situ from the bases of 77 individual stalagmites from 13 caves in southwest Sulawesi indicate that the growth initiation was probably due to wetter conditions (Scroxton et al., 2016), thus suggesting that speleothem growth in Indonesia is a good proxy of hydroclimate. However, the potential of speleothem deposits to reveal late Quaternary major volcanic activities in southern Indonesia has not been fully exploited.

In this study, we investigated two stalagmite samples from the Saripa Cave and Bumi Cave in southern Sulawesi, Indonesia. As this region represents one of the most tectonically active zones on Earth at the junction of three major plate regions with frequent volcanic eruptions and seismicity during the Pleistocene (Hall and Wilson, 2000) (Figures 1A–1C), it is assumed that volcanic eruptions and their environmental responses as well as late Quaternary climate records are simultaneously preserved in the cave deposits. We conducted U-series dating as well as trace element, carbon, oxygen, and strontium isotopic analyses of subsamples taken from individual laminae throughout the stalagmites. The chronology of the $\delta^{18}O$ record for the stalagmite from the Saripa Cave provides both a record of hydroclimatological variations in the Indo-Australian monsoon region (e.g., Griffiths et al., 2009; Ayliffe et al., 2013) and one of abrupt events, which may be ascribed to volcanic eruptions. Dating of the whole stalagmite sample from the Saripa Cave shows that the speleothem growth was not continuous, but occurred in distinct periods, which has been related to the tectonic context here.

2. Tectonic and magmatic setting

Sulawesi is one of the most tectonically active regions in the world because it is the site of interaction of three major lithospheric plates: the Eurasian Plate to the west, the Pacific Plate to the east, and the Australian–Indian Plate to the south (Hall and Wilson, 2000) (Figures 1A–1C). Since the Cretaceous this region has been affected by multiple phases of rifting, subduction magmatism, collision, strike-slip faulting, and rotation, and active deformation continues to the present day. The geology of Sulawesi and the surrounding regions is still not completely understood, and the exact timing of tectonic/volcanic events is not well defined. However, since Indonesia is located along a subduction zone this region is dominated by active volcanoes, with Mount Tambora (in the northern part of Sumbawa) being notable for the most violent eruption in recorded history in 1815. This event caused heavy volcanic ash rains that were observed as far away in Sulawesi (Stothers, 1984). Active volcanoes are also common in North Sulawesi, such as Mount Soputan, which erupted in 2018, emitting ash more than 6000 m into sky (https://phys.org/news/2018-10-volcano-erupts-indonesian-island-earlier.html).

In the Sulawesi region, continent–continent collision and uplift commenced in the early Miocene, related to west dipping subduction and the collision with tectonic blocks derived from the Australian margin. Much of Sulawesi was emergent after the late Miocene, and the present high mountains of west Sulawesi rose in the Pliocene, with active deformation continuing to the present day (Hall and Wilson, 2000).

The modern tectonic regime is dominated by two major NNW-SSE trending wrench faults (Figure 1C; WWF: West Walanae Fault, EWF: East Walanae Fault), which separate the western from the eastern mountains by the Plio-Pleistocene Walanae Graben. The Walanae Fault Zone is a major sinistral strike-slip fault (Guntoro, 1999). Second-order reverse faults observed based on seismic data and stream offsets in the Biru area along the Walanae fault system indicate young lateral movements, although seismic data also support Quaternary normal faulting (van Leeuwen, 1981). The opening of the Walanae Graben was a result of extensional tectonics during the Plio-Pleistocene. Pleistocene volcanic centers with K-rich andesitic and basaltic magmatism occur in South Sulawesi (Figure 1B) (Leterrier et al., 1990). The Saripa Cave (the sample location, see below) was cut in shallow marine carbonate units of the Eocene to Middle Miocene Tonasa Formation (Wilson et al., 2000), which are underlain by Paleocene to Eocene andesitic and trachytic lavas and tuffs and overlain by Miocene to Pliocene predominantly alkaline volcanic rocks (van Leeuwen, 1981).

3. Sample location, modern climate, and material

Saripa Cave (5°2′38.4″S, 119°42′4″E) is located in the Maros limestone district of southwest Sulawesi, Indonesia, near

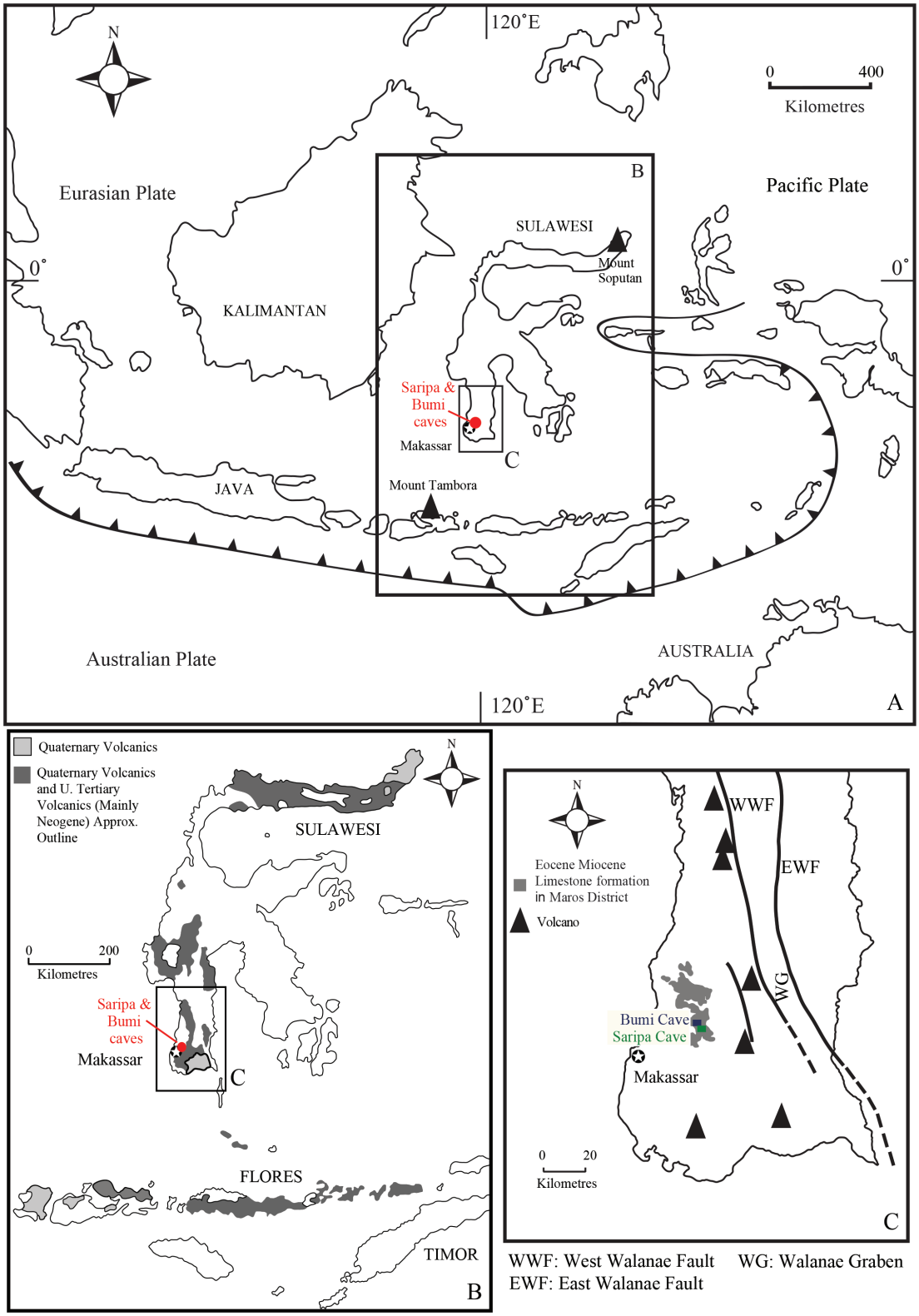

Figure 1. Locations of the studied caves (Saripa and Bumi, colored dots and arrows) in relation to the tectonic setting and Quaternary volcanic eruption centers of Sulawesi. Note the Mount Tambora and Mount Soputan volcanoes that erupted in historical times and produced widespread heavy volcanic ash rains.

the city of Makassar (Figure 1C). The cave is approximately 1.7 km in total length, with two entrances. The main entrance opens 50 m above sea level (cave elevations range from –27 to +32 m a.s.l.) and the stalagmite sample (SR04-ST3 or ST-3) was located 150 m from this entrance in a side passage adjoining a large central chamber (Figure 1). Cave annual mean air temperature is 26 °C and relative humidity >90%. The Asian-Australian Monsoon system, rainfall pattern, seasonal winds, and mean position of the ITCZ are shown in Figure 2. Present-day rainfall around Makassar in SW Sulawesi is strongly seasonal, under the effect of either NW monsoon or SE trades (Figure 2). The rainy season lasts from November to April, dominating during January and December, and it is strongly influenced by changes in the position and intensity of the Walker Circulation and hence by the Indian Ocean Dipole and the El Nino-Southern Oscillation (ENSO; Philander, 1983) events (Figure 2).

High-resolution drilling with 1-mm diamond-tipped burrs attached to a dental drill (5000 rpm) was carried out at 3-mm intervals along the central growth axis of a transect slab of stalagmite sample SR04-ST3, which was precleaned with deionized water and dried in the oven at a temperature of about 50 °C. Burrs were ultrasonically cleaned in distilled water for 3 min after each sample was taken in order to avoid cross-contamination. The stalagmite slab was cleaned of any remaining powder with high-pressure air pulses. A total of 149 powder samples were drilled from SR04-ST3. Seventy-four samples (~230–180 µg) were taken at 6-mm intervals (i.e. every second sample) for C and O isotope ratios analysis. Twenty subsamples (3.1–4.4 mg) were then analyzed for trace element concentrations (ca. 5-cm intervals) and 16 subsamples (5–10 mg) were also selected for Sr (strontium) isotope ratio analysis, focused on areas characterized by dark laminae (Figure 3). Based on the thin section and XRD studies all investigated

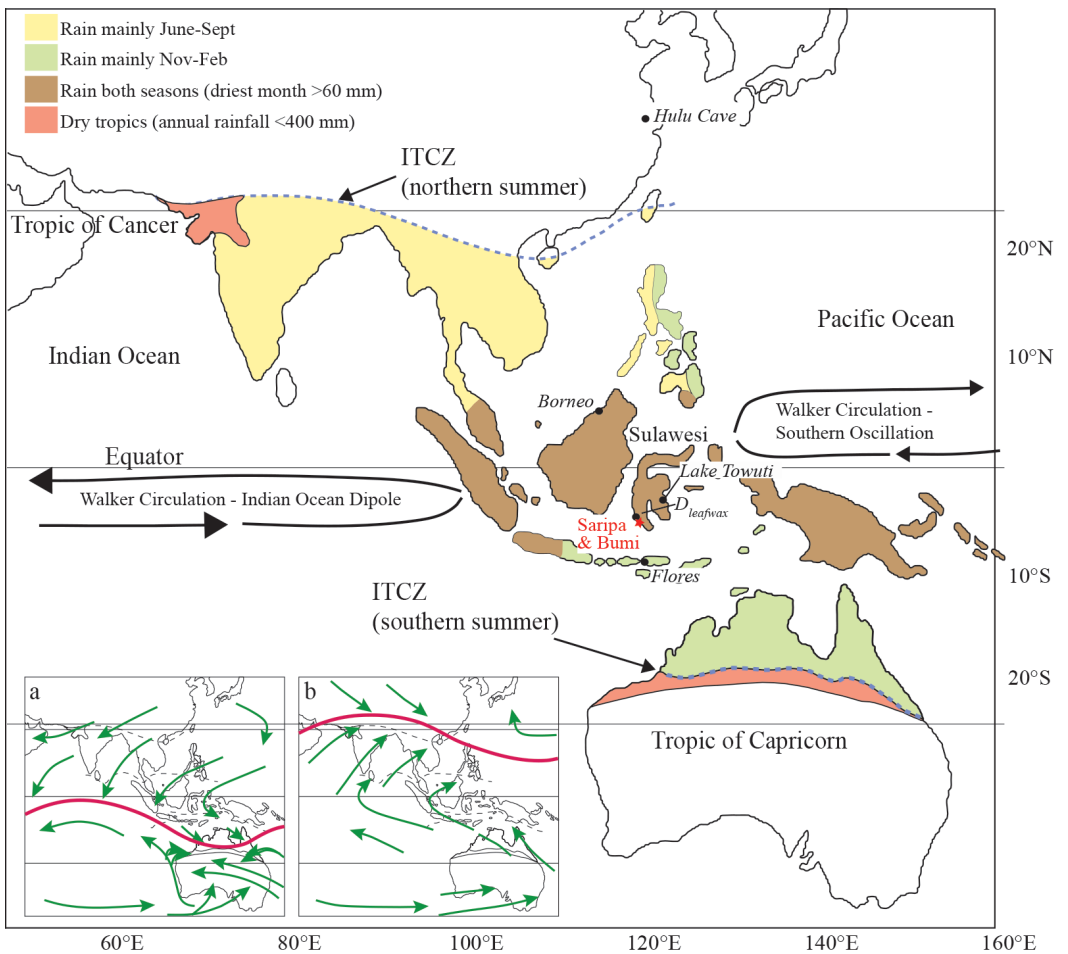

Figure 2. Modern climate of Sulawesi with the Asian-Australian Monsoon system and annual rainfall patterns. Inset: low-level wind circulation for (a) SH summer and (b) NH summer. Black star indicates the locations of the Saripa and Bumi Caves in SW Sulawesi. Black dots are for the locations of the sites discussed in the text (Hulu Cave: Wang et al., 2001; Borneo: Partin et al., 2007; Flores: Griffiths et al., 2009 and Ayliffe et al., 2013; Sulawesi leaf wax: Tierney et al., 2012; Lake Towuti: Russell et al., 2014).

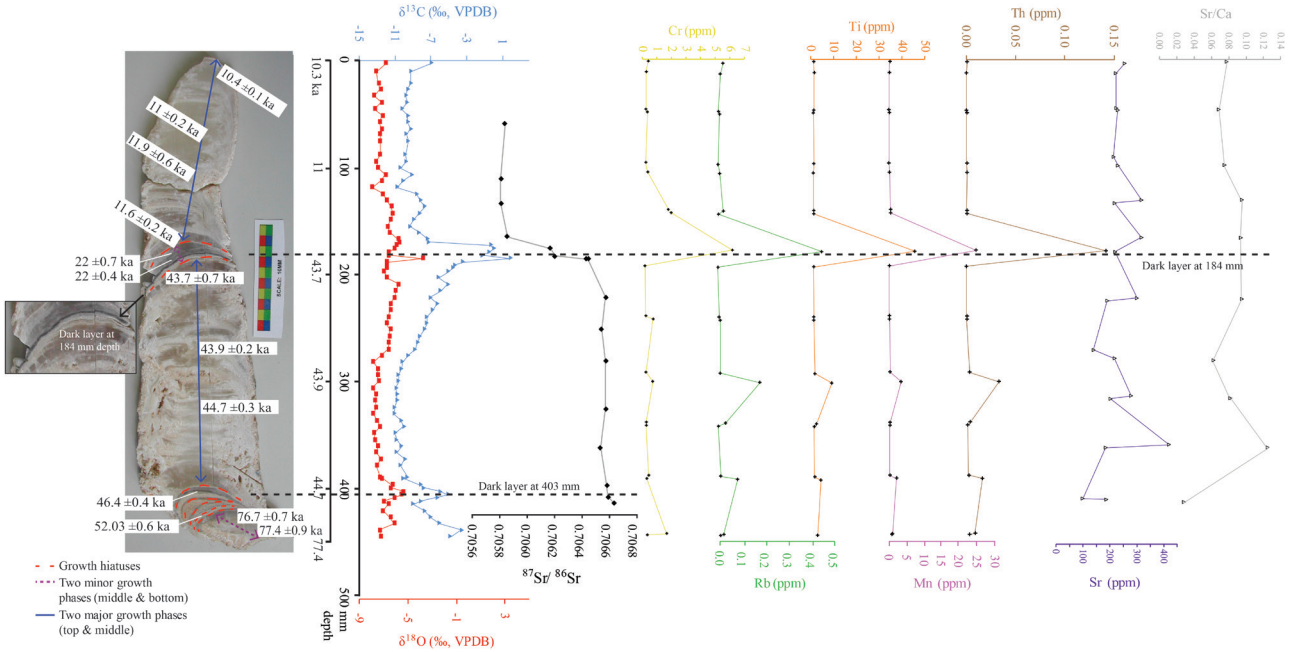

Figure 3. Cross-section of the stalagmite SR04-ST3 (Saripa Cave) showing the growth phases, hiatuses, U-series ages, and contents of some selected trace elements in comparison to stable isotope compositions.

samples including these dark layers are composed of calcite (Figure 4). A total of 12 powder samples (150–330 mg) were drilled (with diamond-tipped burrs, same cleaning procedure as above) for U-series dating. A representative distribution of U/Th samples was taken along the central growth axis of the stalagmite (Figure 3).

Anomalous changes in trace element and isotopic composition were observed in some calcite layers in sample SR04-ST3. We therefore compared the Saripa record with that from another stalagmite sample (BC-09-3-C) collected from Bumi Cave (located about 4 km northwest of the Saripa Cave; Figure 1C), from which the U-series age, trace element, and isotope data were obtained, although not at the same resolution as the Saripa record. Similar to SR04-ST3, a total of 22 powdered samples were microdrilled (using diamond-tipped burrs) from BC-09-3-C. Six samples were selected for the U-series dating, while all of the samples were used for trace element, stable isotope, and Sr isotope analyses (Figure 5).

4. Analytical techniques

U-series dating was carried out on a VG sector-54 thermal ionization mass spectrometer (TIMS) in the Radiogenic Isotope Laboratory at the University of Queensland following the analytical procedures described by Zhao et al. (2001) and Clark et al. (2014). Optically pristine calcite crystals were extracted from each sample, cleaned ultrasonically, and spiked with a ^{229}Th–^{233}U–^{236}U mixed tracer. The ^{233}U–^{236}U double spike with precisely known ^{233}U/^{236}U ratio was used to monitor and correct for U mass-fractionation to improve the analytical precision of the U isotope ratio measurements. After total dissolution in nitric acid, concentrated hydrogen peroxide was added to decompose any organic matter present within the speleothem and to ensure complete mixing between the spike and the sample. U and Th were coprecipitated with iron hydroxide and then redissolved in nitric acid prior to purification using standard anion-exchange methods. The U and Th fractions were loaded onto individual pre-degassed, zone-refined rhenium filaments and sandwiched between two graphite layers. The ^{229}Th, ^{230}Th, ^{232}Th, ^{236}U, ^{234}U, and ^{233}U signals were measured on a Daly ion counter of the TIMS as ^{232}Th/^{229}Th, ^{229}Th/^{230}Th, ^{233}U/^{235}U, ^{234}U/^{235}U, and ^{233}U/^{236}U ratios in peak jumping mode. U and Th concentrations and ^{230}Th/^{238}U and ^{234}U/^{238}U ratios were calculated based on the measured isotope ratios, tracer and sample weights, and isotope concentrations and ratios of the mixed tracer. The ^{230}Th/^{238}U and ^{234}U/^{238}U activity ratios were then calculated using the decay constants of Cheng et al. (2000). The U-series ages (Table 1) were calculated using the Isoplot/Ex version 2 program of Ludwig (2012) and included corrections for nonradiogenic ^{230}Th assuming an average crustal ^{230}Th/^{232}Th atomic ratio of (4.4 ± 2.2) × 10^{-6} for the nonradiogenic component. Further details on analytical procedures and instrumentation were given by Zhao et al. (2001) with further modifications described by Clark et al. (2014). Sr isotopic ratios were also measured by TIMS at the University of Queensland. Sr isotopic ratios

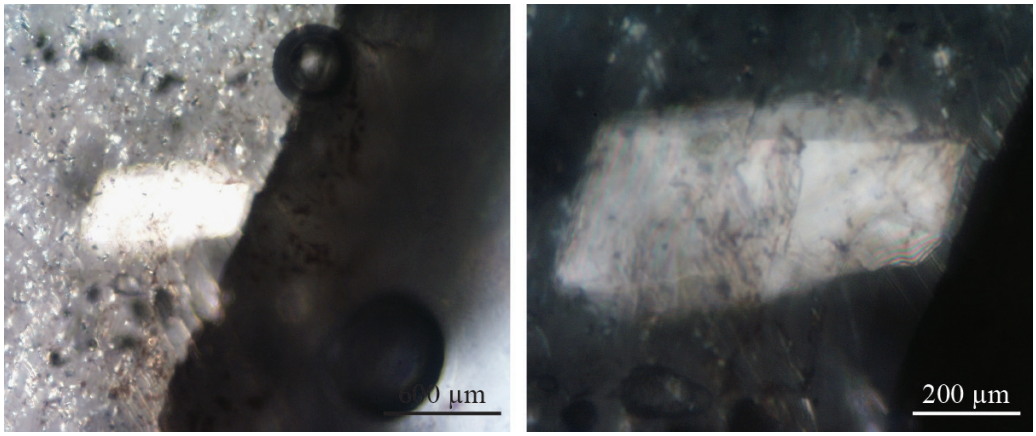

Figure 4. Thin section photos showing the change from light to the dark layers with continuous calcite growth with no structural interruption.

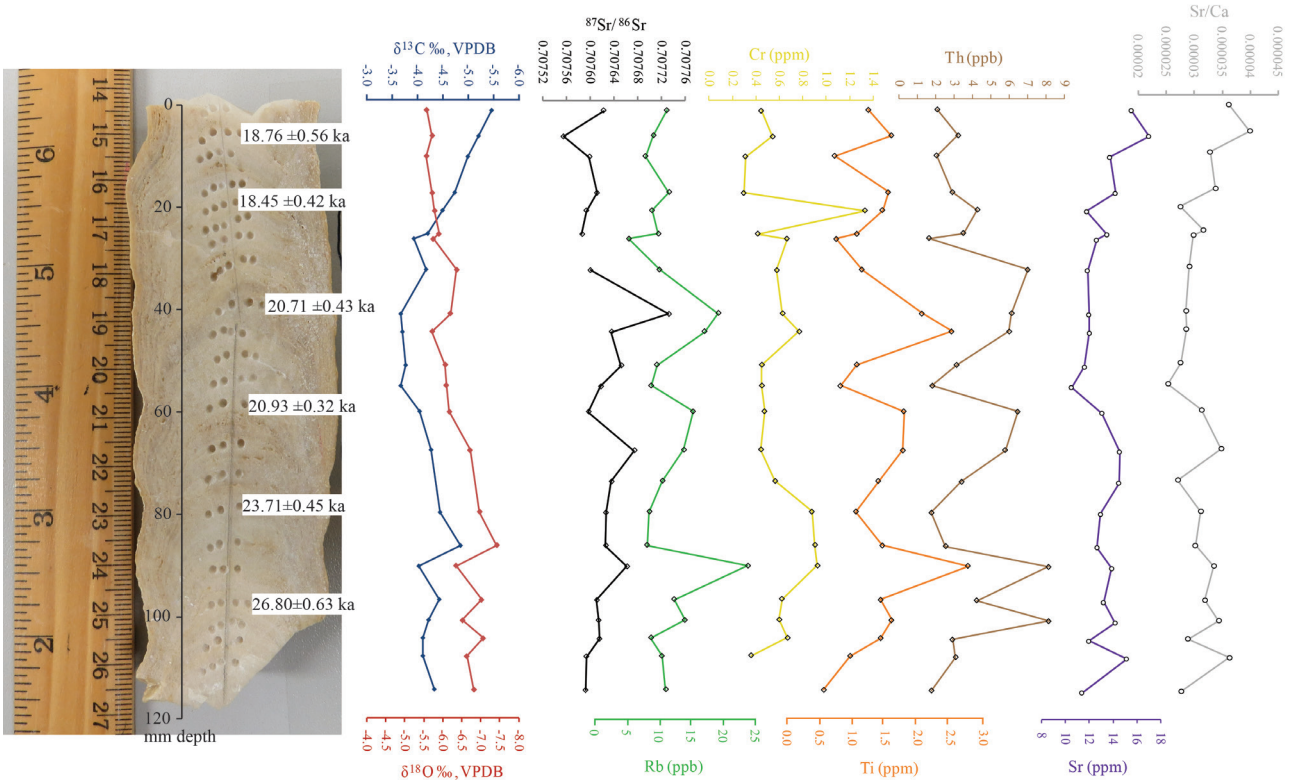

Figure 5. Cross-section of the stalagmite BC-09-3-C (Bumi Cave) showing the growth phases, hiatuses, U-series ages, and contents of some selected trace elements in comparison to stable isotope compositions.

were corrected for mass discrimination using $^{86}Sr/^{88}Sr$ = 0.1194. Long-term repeated analyses of the SRM 987 international standard yielded a mean $^{87}Sr/^{86}Sr$ value of 0.710249 ± 0.000028 (2σ).

For trace element analysis, carbonates were dissolved in a 2% nitric acid solution doped with a multielement internal standard solution. The resulting solutions were analyzed on a Thermo X-series ICP-MS using high-performance sample cones with instrument conditions similar to those described by Lawrence and Kamber (2006). The raw data were corrected for the low but detectable blank, internal and external drifts, and oxides and doubly charged species. Instrument response was calibrated against two independent digests of the USGS reference material W-2 and confirmed by analysis of other reference materials, treated as unknowns.

Table 1. U-Th isotopic data for stalagmites SR04-ST3 and BC-09-3-C.

Sample name	Depth (mm)	U (ppm) ± 2σ	^{232}Th (ppb) ± 2σ	(^{230}Th/ ^{232}Th)	(^{230}Th/ ^{238}U) ± 2σ	(^{234}U/ ^{238}U) ± 2σ	Corr. initial (^{234}U/^{238}U) ± 2σ	Uncorr. ^{230}Th age (ka) ± 2σ	Corr. ^{230}Th age (ka) ±2σ
ST3a	7	0.10084 ± 0.00015	0.235 ± 0.001	122.0	0.0937 ± 0.0008	1.0250 ± 0.0017	1.0258 ± 0.0017	10.49 ± 0.09	10.42 ± 0.09
ST3-090	90	0.19102 ± 0.00019	0.1740 ± 0.0007	328.0	0.0984 ± 0.0015	1.0276 ± 0.0023	1.0284 ± 0.0023	10.95 ± 0.18	10.92 ± 0.18
ST3-127	127	0.20797 ± 0.00025	8.556 ± 0.285	8.60	0.1165 ± 0.0020	1.0272 ± 0.0025	1.0285 ± 0.0027	13.08 ± 0.24	11.89 ± 0.64
ST3-170	170	0.21000 ± 0.00016	0.557 ± 0.007	118.9	0.1039 ± 0.0015	1.0229 ± 0.0016	1.0237 ± 0.0016	11.64 ± 0.18	11.57 ± 0.18
ST3-175	175	0.12572 ± 0.00014	0.300 ± 0.014	243.0	0.1911 ± 0.0052	1.0332 ± 0.0036	1.0354 ± 0.0038	22.22 ± 0.68	22.15 ± 0.68
ST3-180	180	0.09741 ± 0.00019	0.1840 ± 0.0013	307.0	0.1916 ± 0.0026	1.0547 ± 0.0061	1.0582 ± 0.0065	21.76 ± 0.36	21.71 ± 0.36
ST3-200	200	0.20901 ± 0.00017	0.6380 ± 0.0038	339.1	0.3414 ± 0.0041	1.0274 ± 0..0016	1.0310 ± 0.0018	43.83 ± 0.66	43.75 ± 0.66
ST3-310	310	0.47740 ± 0.00040	0.2260 ± 0.0014	2210	0.3450 ± 0.0014	1.0358 ± 0.0020	1.0405 ± 0.0023	43.94 ± 0.24	43.92 ± 0.24
ST3-412	412	0.33179 ± 0.00033	3.131 ± 0.049	115.8	0.3602 ± 0.0019	1.0304 ± 0.0024	1.0348 ± 0.0027	46.66 ± 0.34	46.39 ± 0.37
ST3-430	430	0.90735 ± 0.00068	23.77 ± 0.196	46.28	0.3996 ± 0.0026	1.0366 ± 0.0016	1.0428 ± 0.0018	52.78 ± 0.45	52.03 ± 0.58
ST3-440	440	0.14514 ± 0.00015	1.390 ± 0.026	161.6	0.5115 ± 0.0026	1.0075 ± 0.0028	1.0093 ± 0.0035	76.98 ± 0.67	76.69 ± 0.68
ST3-450	450	0.20813 ± 0.00020	1.560 ± 0.019	208.3	0.5160 ± 0.0038	1.0105 ± 0.0024	1.0131 ± 0.0029	77.60 ± 0.88	77.38 ± 0.89
BC3C-0070	7	0.14834 ± 0.00011	5.750 ± 0.017	14.02	0.1791 ± 0.0015	1.0766 ± 0.0020	1.0817 ± 0.0022	19.83 ± 0.19	18.76 ± 0.56
BC3C-0215	21.5	0.15643 ± 0.00007	4.280 ± 0.011	19.27	0.1738 ± 0.0015	1.0752 ± 0.0016	1.0798 ± 0.0018	19.21 ± 0.19	18.45 ± 0.42
BC3C-0415	41.5	0.17668 ± 0.00009	5.030 ± 0.013	20.57	0.193 ± 0.0015	1.078 ± 0.0013	1.0833 ± 0.0015	21.5 ± 0.19	20.71 ± 0.43
BC3C-0605	60.5	0.18607 ± 0.00009	3.560 ± 0.008	30.56	0.1925 ± 0.0014	1.0768 ± 0.0018	1.082 ± 0.0020	21.45 ± 0.18	20.93 ± 0.32
BC3C-0800	80	0.15529 ± 0.00013	4.610 ± 0.011	22.35	0.2185 ± 0.0016	1.0836 ± 0.0013	1.0901 ± 0.0014	24.52 ± 0.21	23.71 ± 0.45
BC3C-0970	97	0.1242 ± 0.00008	5.660 ± 0.015	16.47	0.2474 ± 0.0011	1.0889 ± 0.0011	1.0971 ± 0.0013	28.04 ± 0.15	26.8 ± 0.63

For $\delta^{13}C$ and $\delta^{18}O$ analyses of SR04-ST3, carbonate powders (~200 mg) were acidified and the evolved CO_2 was analyzed by a Finnigan MAT 251 mass spectrometer equipped with an automated Kiel carbonate reaction device at the Australian National University. Additionally, stalagmite BC-09-3-C (3–4 mg powders) was analyzed for the stable isotope ratios at the University of Queensland, Stable Isotope Geochemistry Laboratory (SIGL) of School of Earth Sciences, on an Isoprime Dual Inlet Isotope Ratio Mass Spectrometer (DI-IRMS) with Multiprep. Samples were reacted with orthophosphoric acid at 90 °C for 1000 s and calibrated against NBS-18 (–5.01‰, –23.01‰ for $\delta^{13}C$ and $\delta^{18}O$, respectively) and NBS-19 (1.95‰, –2.20‰ for $\delta^{13}C$ and $\delta^{18}O$, respectively) international standards. All isotopic ratios are reported in permil (‰) deviations relative to the Vienna Peedee Belemnite (VPDB) standard in the conventional manner, with analytical uncertainties better than ±0.2‰ (2σ) for both $\delta^{13}C$ and $\delta^{18}O$.

5. Results

5.1. U-series dating

U-series age data are presented in Table 1 and the locations of samples with their U-series ages on two stalagmites are shown in Figures 3 and 5. Two major growth phases are evident at the top and middle of investigated stalagmite SR04-ST3: from 10.4 ± 0.1 ka (7 mm) to 11.6 ± 0.2 ka (170 mm) and from 43.8 ± 0.7 ka (200 mm) to 44.7 ± 0.3 ka (398 mm) (Figures 3 and 6). There are also growth phases at the middle and bottom sections of the stalagmite, respectively: from 21.7 ± 0.4 ka (180 mm) to 22.2 ± 0.7 ka (175 mm), at 46.4 ± 0.4 ka (412 mm), at 52 ± 0.6 ka (430 mm), and from 76.7 ± 0.7 ka (440 mm) to 77.4 ± 0.9 ka (450 mm) (Figure 6). Stalagmite SR04-ST3 displays a number of growth hiatuses as well as two optically dark layers, one at ~403 mm and another more prominent one at ~184 mm depth. The Bumi stalagmite (BC-09-3-C) shows continuous growth from 26.80 ± 0.63 ka to 18.45 ± 0.42 ka (Figures 5 and 6; Table 1).

5.2. Trace element, Sr, and stable isotope data

Results for stable isotope and trace element geochemistry for stalagmites SR04-ST3 and BC-09-3-C are given in Table 2 and Table 3, respectively. Trace element data for BC-09-3-C are presented in Table 4. Trace element (Cr, Mn, Rb, Th, Ti, and Sr) concentrations for SR04-ST3 are plotted with $\delta^{18}O$ and $\delta^{13}C$ values in Figure 3. A sharp increase in trace element abundance, which correlates with increasing $\delta^{18}O$ and $\delta^{13}C$ values, is prominent in the optically dark layers (calcite layers) at 184 mm, and slightly at 403 mm (Figure 3). In addition, in the Saripa Cave stalagmite (SR04-ST3), after the appearance of the optically dark layers, $^{87}Sr/^{86}Sr$ values (average: 0.7063) drop to become a plateau although

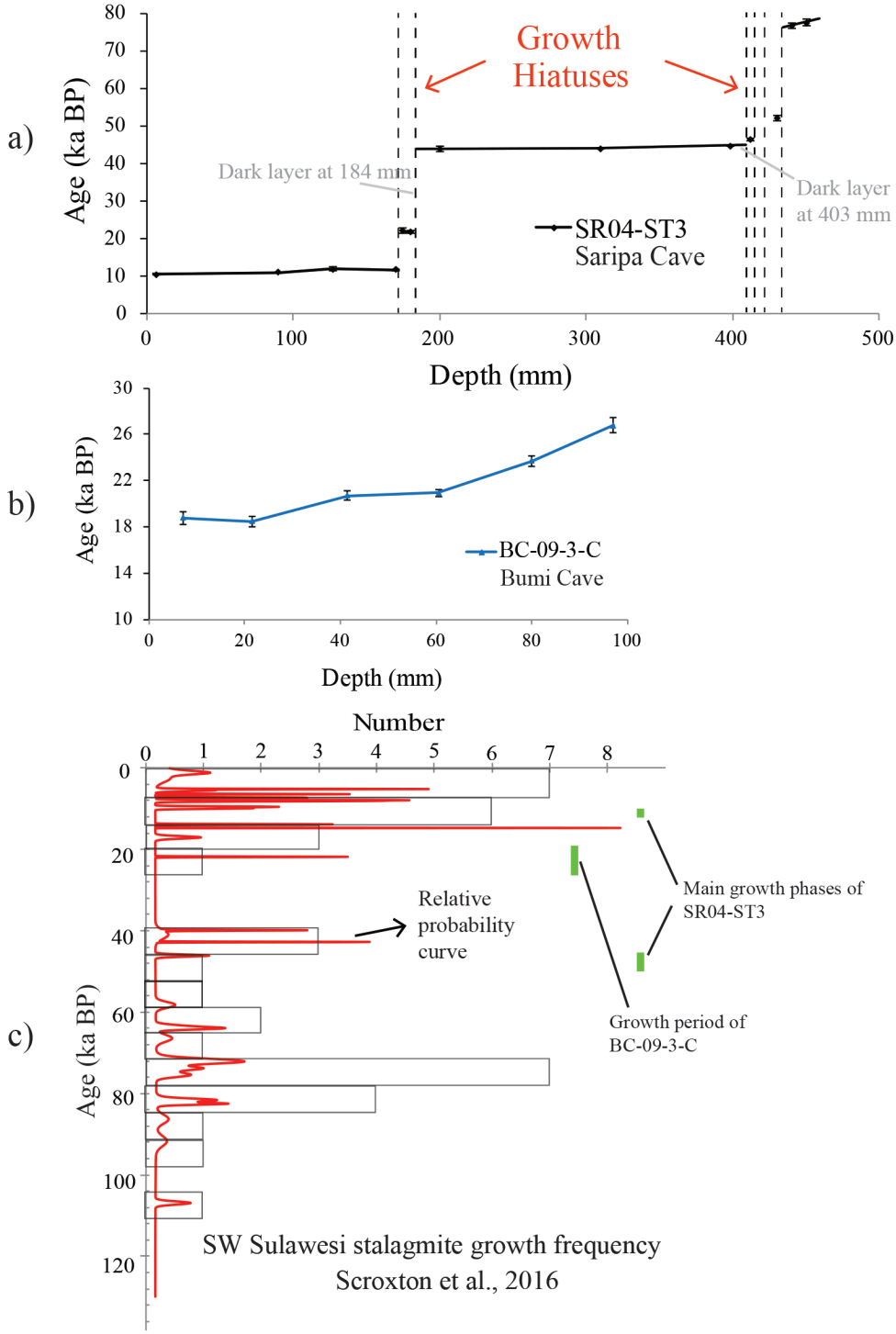

Figure 6. U-series ages vs. depth plots for the stalagmites SR04-ST3 (a) and BC-09-3-C (b). For comparison, stalagmite growth frequency (0–120 ka) in SW Sulawesi (c) (Scroxton et al., 2016) is also shown.

they show a shift (Figure 3). The $^{87}Sr/^{86}Sr$ values (average: ~0.7065) of samples formed between 43.8 ± 0.7 ka and 44.7 ± 0.3 ka following the precipitation of the optically dark layer at 403 mm are low compared to Eocene seawater values ($^{87}Sr/^{86}Sr$ = 0.7077–0.7078) expected in the limestone hosting the cave (Burke et al., 1982; Wilson et al., 2000). Sr isotope values (average: 0.7058) of samples formed from 10.4 ± 0.1 ka to 11.6 ± 0.2 ka following the development of

Table 2. C-O isotope data for stalagmites SR04-ST3 and BC-09-3-C.

Sample ID	Depth (mm)	Age (ka)	$\delta^{13}C$ (‰ VPDB)	$\delta^{18}O$ (‰ VPDB)
SR04-ST3-0025	2.5	10.39	–6.99	–6.81
SR04-ST3-0105	10.5	10.44	–9.28	–7.61
SR04-ST3-0215	21.5	10.51	–9.28	–7.45
SR04-ST3-0270	27	10.54	–9.61	–7.25
SR04-ST3-0330	33	10.58	–9.82	–7.77
SR04-ST3-0390	39	10.61	–9.66	–7.19
SR04-ST3-0450	45	10.65	–10.25	–7.75
SR04-ST3-0515	51.5	10.69	–9.57	–7.12
SR04-ST3-0575	57.5	10.72	–9.59	–7.34
SR04-ST3-0635	63.5	10.76	–9.24	–7.18
SR04-ST3-0690	69	10.79	–9.74	–7.32
SR04-ST3-0750	75	10.83	–9.53	–7.32
SR04-ST3-0880	88	10.90	–9.88	–7.30
SR04-ST3-0940	94	10.95	–9.74	–7.64
SR04-ST3-1000	100	11.00	–10.41	–7.48
SR04-ST3-1060	106	11.05	–9.10	–6.87
SR04-ST3-1120	112	11.10	–10.08	–7.20
SR04-ST3-1180	118	11.15	–10.77	–7.95
SR04-ST3-1240	124	11.19	–8.59	–7.08
SR04-ST3-1300	130	11.24	–8.17	–6.76
SR04-ST3-1360	136	11.29	–7.67	–6.39
SR04-ST3-1420	142	11.34	–8.26	–6.27
SR04-ST3-1480	148	11.39	–8.95	–6.40
SR04-ST3-1540	154	11.44	–9.34	–6.68
SRO4-ST3-1600	160	11.49	–8.34	–6.51
SR04-ST3-1660	166	11.53	–7.35	–5.82
SR04-ST3-1690	169	11.56	–7.23	–5.73
Hiatus#1	171			
SR04-ST3-1715	171.5	21.05	–0.29	–5.96
SR04-ST3-1750	175	21.44	0.02	–6.15
SR04-ST3-1780	178	21.83	–0.54	–6.62
SR04-ST3-1810	181	22.19	–1.29	–6.60
SR04-ST3-1840	184	22.55	1.85	–3.82
SR04-ST3-1870	187	22.91	–3.44	–6.74
Hiatus#2	187			
SR04-ST3-1900	190	43.73	–4.30	–6.79
SR04-ST3-1930	193	43.74	–4.59	–6.77
SR04-ST3-1960	196	43.74	–5.06	–6.96
SR04-ST3-2020	202	43.75	–6.14	–6.74
SR04-ST3-2080	208	43.76	–5.11	–5.76
SR04-ST3-2140	214	43.77	–5.91	–6.01

Table 2. (Continued).

SR04-ST3-2200	220	43.78	–7.07	–6.10
SR04-ST3-2260	226	43.79	–6.30	–6.46
SR04-ST3-2320	232	43.80	–6.78	–6.44
SR04-ST3-2380	238	43.81	–7.48	–6.64
SR04-ST3-2440	244	43.82	–7.46	–6.78
SR04-ST3-2500	250	43.83	–7.73	–6.45
SR04-ST3-2560	256	43.84	–8.20	–6.54
SR04-ST3-2620	262	43.85	–8.48	–6.57
SR04-ST3-2680	268	43.86	–8.80	–6.60
SR04-ST3-2740	274	43.87	–9.56	–7.18
SR04-ST3-2800	280	43.88	–10.18	–7.87
SR04-ST3-2860	286	43.89	–10.30	–7.47
SR04-ST3-2920	292	43.90	–10.61	–7.52
SR04-ST3-2980	298	43.91	–10.60	–7.42
SR04-ST3-3040	304	43.87	–10.91	–7.90
SR04-ST3-3100	310	43.92	–10.81	–7.62
SR04-ST3-3160	316	43.98	–10.80	–7.71
SR04-ST3-3220	322	44.03	–11.08	–7.61
SR04-ST3-3280	328	44.08	–11.09	–7.87
SR04-ST3-3340	334	44.13	–10.35	–7.54
SR04-ST3-3400	340	44.19	–10.05	–7.32
SR04-ST3-3460	346	44.24	–10.98	–7.78
SR04-ST3-3520	352	44.29	–10.84	–7.75
SR04-ST3-3580	358	44.34	–10.30	–7.47
SR04-ST3-3640	364	44.39	–10.85	–7.63
SR04-ST3-3700	370	44.45	–9.92	–7.23
SR04-ST3-3760	376	44.50	–10.39	–7.58
SR04-ST3-3870	387	44.59	–9.63	–7.29
SR04-ST3-3880	388	44.60	–10.14	–7.14
SR04-ST3-3940	394	44.66	–8.19	–6.31
SR04-ST3-3970	397	44.68	–7.78	–6.44
SR04-ST3-4000	400	44.71	–5.98	–5.38
SR04-ST3-4030	403	44.73	–5.14	–5.52
SR04-ST3-4060	406	44.76	–6.32	–6.11
Hiatus#3	409			
SR04-ST3-4090	409	46.20	–8.09	–6.97
SR04-ST3-4120	412	46.39	–8.98	–6.64
Hiatus#4	415			
SR04-ST3-4180	418	48.39	–7.72	–7.05
Hiatus#5	422			
SR04-ST3-4240	424	50.39	–7.00	–6.45
Hiatus#6	426.5			
SR04-ST3-4300	430	52.03	–6.04	–6.15

Table 2. (Continued).

Hiatus#7	430			
Hiatus#8	433			
SR04-ST3-4360	436	76.42	–3.61	–7.35
SR04-ST3-4420	442	76.83	–4.86	–7.24
BC3C-0020	2	17.25	–5.46	–5.58
BC3C-0070	7	18.76	–5.21	–5.72
BC3C-0110	11	18.04	–5.00	–5.56
BC3C-0180	18	18.65	–4.73	–5.72
BC3C-0215	21.5	18.45	–4.50	–5.79
BC3C-0260	26	19.35	–4.20	–5.90
BC3C-0270	27	19.44	–3.93	–5.75
BC3C-0330	33	19.96	–4.18	–6.36
BC3C-0415	41.5	20.71	–3.67	–6.20
BC3C-0450	45	21.02	–3.71	–5.72
BC3C-0515	51.5	21.58	–3.77	–6.07
BC3C-0555	55.5	21.93	–3.67	–6.10
BC3C-0605	60.5	20.93	–4.04	–6.18
BC3C-0680	68	23.03	–4.27	–6.72
BC3C-0800	80	23.71	–4.45	–6.97
BC3C-0865	86.5	24.65	–4.85	–7.42
BC3C-0905	90.5	25.00	–4.02	–6.35
BC3C-0970	97	26.80	–4.42	–7.02
BC3C-1010	101	25.92	–4.22	–6.51
BC3C-1045	104.5	26.23	–4.11	–7.06
BC3C-1080	108	26.53	–4.11	–6.63
BC3C-1145	114.5	27.10	–4.34	–6.82

Age models were obtained using the Excel Forecast function.

the optically dark layer at 184 mm are even lower (Figure 3). Low Sr isotope values are characteristic of Sr sourced from young volcanic materials (Burke et al., 1982). In comparison to SR04-ST3, O (–7‰ to –5‰, VPDB), C (–5‰ to ‰3‰, VPDB), and Sr isotopic compositions and trace element contents of the Bumi stalagmite have not changed significantly during the entire growth history (Figure 5). In particular, $^{87}Sr/^{86}Sr$ values are much higher than those for SR04-ST3, with a narrow range between 0.7075 and 0.7077 (Figure 5; Table 5).

5.3. Hendy tests

Hendy tests (Hendy, 1971) were conducted to determine if the stalagmite SR04-ST3 was deposited in quasi-isotopic equilibrium. Multiple samples were taken from 6 separate growth layers along the length of the stalagmite (4 samples per layer) for the Hendy test (Figure 7). Isotopic values are plotted as distances away from the central growth axis (Figure 7). Nonequilibrium fractionation during deposition may have occurred if $\delta^{18}O$ along single growth layers varies by more than 0.5‰ (Hendy, 1971) or if sampling of the same lamina was not possible. Our results indicate that $\delta^{18}O$ values have not varied by more than 0.5‰ along the majority of tested growth layers, except for subsamples at 250 mm (Figure 7). The results of these Hendy tests imply that the stalagmite SR04-ST3 calcite was likely deposited at quasi-isotopic equilibrium, suggesting slow degassing of CO_2 from drip waters. The Hendy test shows that within-layer $\delta^{18}O$ variation is less than 0.5‰, significantly smaller than the overall magnitudes of change across the entire record. Even for the optically dark layers, the variation within a single growth layer is considerably smaller than the temporal variability. This supports the notion that the optically dark layers were also formed in isotope equilibrium.

6. Discussion and interpretation

6.1. Growth hiatuses and phases in SR04-ST3

While growth interruptions could be related to many causes including changes in cave plumbing, exceptionally dry or wet (flooding) climate, and/or variations in the chemistry of seepage water, the growth of stalagmites is commonly a result of relatively humid periods (Scroxton et al., 2016) (see also Figure 6). As mentioned above, SR04-ST3 shows two major and three minor growth phases. The speleothem growth at 10.4–11.6, as presented with $\delta^{18}O$ values in Figure 8, occurred at times correlated with a strong northern hemisphere (NH) summer monsoon as recorded in Hulu Cave (Wang et al., 2001), whereas growth phases (presented with $\delta^{18}O$ values in Figure 9) dated at 43.8–44.7 ka coincided with NH dry (weaker NH summer monsoon) periods (St Pierre et al., 2007). However, growth phases in SR04-ST3 do not coincide with positive anomalies in stalagmite growth frequency, which is reported for 77 individual stalagmite samples from thirteen caves in the same area (Scroxton et al., 2016) (Figure 6). This suggests that nonclimatic factors likely affected the continuous growth of speleothems in the Saripa Cave during growth phases documented in SR04-ST3 (see the discussion below).

6.2. Stable isotope data

When precipitating in quasi-isotope equilibrium, the oxygen isotope ratios of stalagmite carbonate are a function of the $\delta^{18}O$ of the film of fluid from which the crystals precipitated and the cave temperature, which approximates the annual mean surface air temperature. In monsoon-dominated, low-latitude, and tropical regions, temperature effects are commonly insignificant and much smaller than the rainfall amount effect because of the small temperature dependence of the oxygen isotope fractionation between

Table 3. ICP-MS trace element data (in ppb) for stalagmite SR04-ST3.

Sample ID	3-0025	2-130	2-490	3-515	2-1000	3-1090	3-1450	2-1480	3-1840	32905	3-2470.	2500	3010	3-3100.	3-3490.	3520	3-4000.	4030	3-4560.	4570
Depth (mm)	2.5	13.0	49.0	52	100.0	109.0	145.0	148.0	184.0	199.0	247.0	250.0	301.0	310.0	349.0	352.0	400.0	403.0	456.0	457.0
Li	46.53	33.51	21.99	47	24.30	42.57	39.32	19.45	216.34	15.13	41.26	33.26	36.90	77.29	32.97	25.98	42.57	48.37	52.46	u.d.l.
Ti	1373	1582	1524	1284	1467	1202	1315	1313	45604	1393	1505	1513	1970	9330	2712	1590	1856	4602	3163	2113
V	49.26	49.85	47.13	57	58.28	70.83	93.61	65.41	2413.17	53.44	34.83	60.05	105.20	607.7	112.9	79.73	64.32	332.5	128.9	98.31
Cr	387	258	239	338	221	357	1775	1956	6157	179	224	721	243	706	262	255	422	290	1671	332
Mn	304	142	124	193	127	262	480	495	24632	176	159	286	400	3533	396	357	350	2261	1111	869
Co	1358	1395	1846	1477	1424	1484	1602	1466	1645	1642	1265	1345	1418	1528	1395	1528	1519	1573	1663	1677
Ni	9377	12362	186056	8388	9242	10979	78256	95301	8670	6836	8788	57365	12672	9997	7768	6805	21233	8088	33525	9486
Cu	1824	2179	2249	1723	2271	1565	1937	2266	3213	3038	1901	2243	2547	6542	2166	2322	1395	3192	4599	2626
Zn	3639	2335	1787	9268	1371	2168	8889	2028	12301	2188	2841	1977	1764	7547	1896	1901	34744	3939	9161	1896
Rb	24.40	12.49	4.63	9	2.89	10.64	26.12	4.60	455.34	2.04	7.52	12.46	12.37	185.2	34.77	4.69	15.24	88.10	28.28	13.46
Sr	255184	222159	223518	229317	213570	230209	317697	217516	317195	219635	300599	189554	138968	217801	279211	202169	419778	184517	98777	186221
Y	11.60	13.23	14.73	9	23.44	8.70	9.48	20.43	330.06	13.70	10.49	14.22	20.44	58.13	15.64	27.27	14.73	45.66	16.01	50.88
Zr	34.66	23.12	15.14	80	373.81	592.49	27.62	60.14	1120.81	23.12	158.2	67.38	56.34	402.2	67.04	31.94	54.10	133.2	77.10	107.8
Nb	0.83	0.46	0.22	0	0.54	0.69	0.86	0.65	50.51	1.36	0.43	0.62	0.96	9.16	1.04	0.64	0.92	3.52	2.30	1.07
Ba	18511	13709	14689	19669	14475	17436	36710	16092	29868	16225	20298	13213	7951	15740	18981	15099	40329	13145	10696	15523
La	1.89	u.d.l.	0.09	0	0.55	2.59	0.86	0.02	353.6	u.d.l.	0.60	0.41	8.44	65.65	9.38	2.62	4.18	38.51	18.90	8.12
Ce	5.49	1.05	0.94	5	1.04	4.78	1.71	0.70	804.6	0.33	1.57	1.73	19.69	151.9	22.31	5.47	9.91	96.08	41.47	16.98
Pr	0.45	u.d.l.	u.d.l.	u.d.l.	0.02	0.53	0.13	u.d.l.	104.8	u.d.l.	0.01	u.d.l.	2.14	17.49	2.68	0.61	0.99	14.83	4.40	1.91
Nd	4.05	1.48	0.86	2	1.02	2.40	1.53	0.97	383.9	0.66	1.34	1.44	8.73	67.69	10.70	4.54	6.02	46.93	18.58	10.49
Sm	u.d.l	u.d.l.	u.d.l.	u.d.l.	u.d.l.	0.19	u.d.l.	u.d.l.	85.53	u.d.l.	u.d.l.	u.d.l.	1.12	15.01	1.29	u.d.l.	u.d.l.	9.22	3.31	1.51
Eu	u.d.l	u.d.l.	u.d.l.	0	0.06	0.29	0.48	0.01	23.07	u.d.l.	0.24	u.d.l.	0.04	4.20	0.54	u.d.l.	0.36	2.15	1.02	0.17
Tb	0.40	0.41	0.26	0	0.23	0.25	0.18	0.16	10.99	0.17	0.22	0.35	0.44	2.01	0.43	0.30	0.34	1.51	0.70	0.48
Gd	5.19	5.35	3.09	4	1.94	2.62	2.38	1.77	83.17	1.52	4.02	5.79	5.46	16.57	4.13	3.85	2.53	11.52	5.43	3.97
Dy	8.85	9.12	5.24	7	4.33	4.32	2.96	4.00	61.30	2.63	5.88	9.85	8.59	14.66	4.41	6.01	4.56	10.16	4.97	6.28
Ho	0.16	0.19	0.11	0	0.26	0.06	0.07	0.17	12.12	0.11	0.09	0.21	0.38	2.08	0.30	0.38	0.19	1.52	0.47	0.79
Er	0.35	0.16	0.33	0	0.94	0.33	0.30	0.52	36.18	0.50	0.06	0.20	1.15	5.39	0.78	1.15	0.37	3.56	1.18	2.70
Tm	0.67	0.54	0.53	1	0.73	0.60	0.67	0.68	5.01	0.62	0.49	0.67	0.74	1.27	0.63	0.86	0.63	1.07	0.88	0.93
Yb	0.34	0.21	0.36	0	0.99	0.38	0.50	0.86	27.83	0.39	0.43	0.41	0.88	4.73	1.18	1.40	0.62	4.01	1.09	2.52
Lu	0.08	0.07	0.06	0	0.13	0.04	0.04	0.15	4.07	0.06	0.01	0.05	0.12	0.67	0.09	0.19	0.09	0.51	0.20	0.42
Hf	0.88	4.47	1.01	2	8.73	14.70	0.66	0.90	33.60	0.64	2.87	1.58	0.77	9.44	1.55	0.69	0.83	6.04	1.87	1.51
Ta	0.06	0.10	0.05	0	0.00	0.05	0.10	0.05	5.28	u.d.l.	0.05	0.02	0.02	0.76	0.12	0.03	0.08	0.21	0.36	0.05
Pb	30.22	763.7	504.2	36	462.6	28.91	23.57	1327	725.3	861.2	23.35	554.0	310.3	138.3	32.53	76.19	47.21	2247	63.09	113.1
Th	0.61	0.07	0.06	0	0.24	0.75	0.19	0.31	141.2	0.08	0.24	0.31	3.30	32.88	3.79	1.16	2.32	16.24	8.70	2.87
U	125.0	277.3	252.0	187	254.0	221.1	283.6	264.6	578.0	244.6	438.4	271.3	355.5	878.3	542.4	274.7	184.2	269.9	246.6	254.0
Ce/Yb	15.95	4.97	2.59	11	1.06	12.50	3.44	0.81	28.91	0.84	3.63	4.18	22.27	32.08	18.85	3.90	16.08	23.94	37.99	6.74
46Ca	3292217			3368669		3060132	3340563		3385558		3153769			3500732	3415208		3366742		3519003	

Table 4. ICP-MS trace element data (in ppb) for stalagmite BC-09-3-C.

Sample ID	BC3C-0020	BC3C-0070	BC3C-0110	BC3C-0180	BC3C-0215	BC3C-0260	BC3C-0270	BC3C-0330	BC3C-0415	BC3C-0450	BC3C-0515	BC3C-0555	BC3C-0605	BC3C-0680	BC3C-0740	BC3C-0800	BC3C-0865	BC3C-0905	BC3C-0970	BC3C-1010	BC3C-1045	BC3C-1080	BC3C-1145
Depth (mm)	2	7	11	18	21.5	26	27	33	41.5	45	51.5	55.5	60.5	68	74	80	86.5	90.5	97	101	104.5	108	114.5
Li	55.78	35.80	17.17	28.00	46.85	36.70	40.45	32.89	56.24	31.98	30.02	4.10	3.10	32.78	322.59	1.09	7.26	13.54	u.d.l.	2.81	18.57	4.73	u.d.l.
Ti	1253	1603	743	1557	1468	1083	759	1160	2073	2523	1076	834	1798	1776	1411	1063	1462	2779	1440	1610	1438	978	576
V	48.70	74.29	44.43	80.30	132.78	51.13	75.67	81.97	105.08	125.17	51.32	56.44	131.96	84.07	64.38	109.38	166.02	149.53	76.43	83.21	59.78	61.76	78.90
Cr	446	541	309	296	1330	418	664	575	627	770	448	449	473	442	562	877	901	926	623	597	669	361	2343
Co	179	182	177	181	183	185	185	182	241	198	187	190	188	196	252	194	206	196	190	196	199	201	194
Ni	2843	3251	3161	3072	2875	3931	3204	2932	8247	3531	2916	3020	3551	2846	3901	2991	5316	3064	6221	2939	3097	3032	3186
Cu	604	810	2221	3871	519	1866	652	1856	7914	3781	583	823	5497	790	1055	518	22009	7182	10378	993	3480	14203	31313
Zn	2870	2640	2722	3501	1152	1900	2379	2473	8194	4630	1384	7826	4852	3899	2316	2283	12831	8137	8102	5880	3238	9900	23874
Rb	11.40	9.24	8.06	11.71	9.07	10.04	5.44	10.22	19.34	17.26	9.82	8.94	15.45	13.99	10.65	8.64	8.29	23.97	12.51	14.21	8.89	10.58	11.21
Sr	15490	17000	13716	14185	11764	13444	12613	11842	11948	11980	11589	10505	13040	14547	14469	12929	12642	13867	13183	14161	11967	15128	11365
Y	10.43	12.85	9.09	13.73	10.23	19.14	7.58	19.40	26.77	33.03	13.09	9.84	25.66	20.97	15.15	8.36	9.97	26.88	19.29	23.33	14.79	17.83	13.96
Zr	30.69	45.38	43.23	38.79	36.95	45.60	31.55	47.96	72.63	72.54	45.71	34.95	69.90	73.17	47.35	33.87	33.19	85.43	43.21	68.21	36.48	43.71	20.06
Nb	4.83	2.31	1.15	2.50	6.67	2.13	2.04	1.86	2.85	2.69	1.60	5.78	7.08	2.79	2.49	1.03	1.75	6.17	2.91	4.02	1.99	1.02	0.46
Ba	1335	680	1031	585	608	484	526	462	524	508	444	374	583	791	444	412	698	881	581	901	412	577	560
La	12.59	17.10	11.44	14.26	17.03	16.02	10.08	16.43	26.91	25.43	14.05	9.39	28.45	26.34	16.49	10.65	11.78	44.98	22.88	25.16	16.07	17.25	13.97
Ce	29.47	35.26	27.99	30.93	31.73	33.17	30.16	59.93	53.14	53.31	33.78	28.26	60.21	59.10	34.00	21.57	25.12	78.72	43.31	53.69	29.81	29.55	20.85
Pr	2.47	3.72	2.29	3.03	3.63	3.62	2.34	3.90	5.98	6.21	3.17	2.22	6.03	5.63	3.73	2.53	2.45	9.28	5.42	6.36	3.84	4.30	2.73
Nd	9.47	15.65	9.28	12.65	14.50	14.92	10.04	16.43	24.00	23.55	13.02	9.33	25.72	22.37	12.98	8.90	10.30	37.70	24.80	46.94	17.64	83.55	37.48
Sm	2.42	2.94	2.55	2.95	2.90	2.90	1.82	3.55	5.30	6.28	2.70	2.25	5.30	5.19	2.89	2.25	1.95	6.98	4.16	5.21	3.34	3.00	2.16
Eu	0.59	0.80	0.59	0.88	0.81	0.90	0.50	1.06	1.41	1.61	0.92	0.57	1.55	1.49	0.86	0.52	0.68	1.73	1.13	1.32	0.92	1.07	0.80
Tb	0.21	0.35	0.28	0.44	0.35	0.43	0.21	0.50	0.69	0.84	0.40	0.16	0.66	0.58	0.42	0.15	0.22	0.91	0.58	0.72	0.37	0.49	0.37
Gd	2.29	2.86	1.98	2.13	2.44	3.26	1.81	4.28	4.10	5.49	2.08	1.52	5.06	4.02	3.00	2.18	1.97	5.49	3.70	3.96	3.45	3.14	1.99
Dy	1.66	2.16	1.26	2.29	1.44	2.93	0.88	2.91	4.18	4.23	1.53	1.34	3.43	3.12	2.19	1.17	1.25	5.13	2.89	3.73	2.47	2.72	1.62
Ho	0.39	0.35	0.23	0.36	0.29	0.58	0.16	0.43	0.74	1.03	0.37	0.27	0.71	0.56	0.57	0.20	0.33	0.80	0.54	0.80	0.43	0.50	0.36
Er	1.10	1.00	0.96	1.29	0.81	1.36	0.59	1.63	2.34	2.94	2.39	0.93	2.14	2.09	1.53	0.75	1.11	2.41	1.51	2.02	1.42	1.34	1.60
Tm	0.17	0.16	0.07	0.12	0.14	0.21	0.10	0.22	0.31	0.39	0.10	0.09	0.29	0.21	0.17	0.08	0.13	0.24	0.11	0.18	0.12	0.20	0.20
Yb	0.71	1.36	0.55	1.34	1.26	1.33	0.60	1.43	2.07	2.67	0.93	0.65	1.83	1.72	1.06	0.52	0.60	1.59	1.14	1.79	1.05	1.37	1.16
Lu	0.10	0.13	0.07	0.12	0.13	0.19	0.12	0.18	0.24	0.32	0.13	0.11	0.25	0.18	0.15	0.11	0.07	0.21	0.15	0.38	0.14	0.14	0.16
Hf	0.93	1.40	1.35	1.21	1.22	1.23	0.89	1.25	1.92	2.25	1.23	0.76	1.70	2.06	1.22	0.79	0.82	2.54	1.10	1.89	0.87	1.15	0.55
Ta	0.61	0.54	2.51	4.05	0.36	0.15	2.19	0.12	0.70	0.17	0.11	32.98	2.07	0.24	0.63	0.40	0.51	0.39	1.15	6.51	1.04	0.42	0.21
Pb	53.37	106	237	449	58.47	81.76	70.58	68.63	360	194	46.86	151	200	100	104	40.96	640	228	517	85.04	150	665	1094
Th	2.06	3.21	2.05	2.90	4.25	3.49	1.64	7.02	6.13	5.99	3.12	1.80	6.46	5.78	3.39	1.74	2.52	8.13	4.23	8.15	2.92	3.06	1.75
U	154	144	150	156	162	174	160	155	160	181	192	161	171	144	230	136	132	121	123	140	148	142	186
^{43}Ca	428128458	426050026	417952040	420059672	427967684	424549899	423245836	406999222	419003152	418751255	419953733	415767758	416940976	418037658	534522466	414663464	418251327	414153169	413647139	411889515	414923464	417286407	410522582

Table 5. Sr isotope data for stalagmites SR04-ST3 and BC-09-3-C.

Sample name	Depth (mm)	$^{87}Sr/^{86}Sr \pm 2\sigma$
ST3-0590	59	0.705796 ± 6
ST3-1100	110	0.705764 ± 6
ST3-1330	133	0.705763 ± 5
ST3-1640	164	0.705814 ± 6
ST3-1750	175	0.706134 ± 6
ST3-1820	182	0.706169 ± 6
ST3-1850a	185	0.706406 ± 7
ST3-1850b	185	0.706418 ± 6
ST3-2200	220	0.706550 ± 6
ST3-2500	250	0.706518 ± 6
ST3-2800	280	0.706550 ± 7
ST3-3240	324	0.706548 ± 7
ST3-3600	360	0.706512 ± 6
ST3-3950	395	0.706559 ± 6
ST3-4060	406	0.706568 ± 6
ST3-4120	412	0.706615 ± 5
BC3C-0020	2	0.707650 ± 5
BC3C-0070	7	0.707582 ± 4
BC3C-0110	11	0.707625 ± 4
BC3C-0180	18	0.707638 ± 4
BC3C-0215	21.5	0.707620 ± 4
BC3C-0260	26	0.707613 ± 4
BC3C-0270	27	0.709727 ± 4
BC3C-0330	33	0.707627 ± 6
BC3C-0415	41.5	0.707759 ± 4
BC3C-0450	45	0.707663 ± 4
BC3C-0515	51.5	0.707679 ± 4
BC3C-0555	55.5	0.707644 ± 4
BC3C-0605	60.5	0.707624 ± 4
BC3C-0680	68	0.707701 ± 4
BC3C-0740	74	0.707662 ± 4
BC3C-0800	80	0.707654 ± 4
BC3C-0865	86.5	0.707653 ± 6
BC3C-0905	90.5	0.707689 ± 5
BC3C-0970	97	0.707638 ± 4
BC3C-1010	101	0.707641 ± 4
BC3C-1045	104.5	0.707643 ± 4
BC3C-1080	108	0.707620 ± 5
BC3C-1145	114.5	0.707619 ± 4

water and calcite (–0.24‰/°C; Friedman and O'Neil, 1977). Modern rainfall $\delta^{18}O$ at Liang Luar on Flores 4° south in latitude of the study site revealed that summer monsoon rainwater is depleted in ^{18}O by 6‰–7‰ in comparison to the rainwater ^{18}O of the rest of the year (Griffith et al., 2009; Ayliffe et al., 2013). This significant change in $\delta^{18}O$ of rainfall on Flores is interpreted as primarily reflecting the change in Asian summer monsoon rainfall amount and the effect of seasonality of rainfall. Similarly, modern rainfall data from Makassar gathered in 2005 show that summer rainfall $\delta^{18}O$ is modestly depleted with averages around –7.09‰ (SMOW) (Gavin Dunbar and Halmar Halide, pers. comm.), although there are no data recorded for the months of October, September, August, and June.

The volume of rainfall (amount effect) is widely interpreted as a control on the isotopic composition of speleothems as the variations of $\delta^{18}O$ in precipitation will be reflected in speleothem calcite (Dansgaard, 1964). Currently the Saripa Cave receives dominantly summer monsoonal rainfall, and changes in the amount of summer rainfall can produce a shift in the $\delta^{18}O$ of Makassar rainfall (Gavin Dunbar and Halmar Halide, pers. comm.). In addition to rainfall amount, seasonality changes between summer monsoon rain and dry season trade wind-induced rain are important, as trade wind-derived rains should be isotopically more depleted. It is also likely that the source regions of the rainfall have changed on longer-term timescales such as glacial-interglacial cycles. In fact, southward progression of the ITCZ during the Last Glacial Maximum (LGM) might have resulted in changes of the moisture source area from a NW monsoon to a SE monsoon in the study region (Ayliffe et al., 2013). A recent study of a Sumatran speleothem demonstrated $\delta^{18}O$ changes (approximately –8‰ to –5‰) that are explained by the changes in rainfall amount and moisture sources with a marked enrichment during the Younger Dryas (YD; Wurtzel et al., 2018). Speleothem response indicates a weakening of moisture transport along both the boreal and austral monsoonal pathways in relation to both southward migrations of the ITCZ and the reduction of Indian Ocean-sourced rainfall.

$\delta^{13}C$-$\delta^{18}O$ values of the Saripa Cave record seem to correlate positively (Figures 3 and 10), which might be related to the climatic and ecological factors (Quade et al., 1989; Burns et al., 2002; Mattey et al, 2008). Positive $\delta^{18}O$ and $\delta^{13}C$ correlation without any kinetic effects for soil carbonates is attributed to effects of evaporation controlling the $\delta^{18}O$ of the soil water (before carbonate formation), and soil respiration rate, moisture, and biomass affecting soil CO_2 and hence the $\delta^{13}C$ of soil carbonates (Quade et al., 1989). Carbon isotope composition together with oxygen isotopes of speleothem carbonates has been reported to be a climate indicator. For example, more

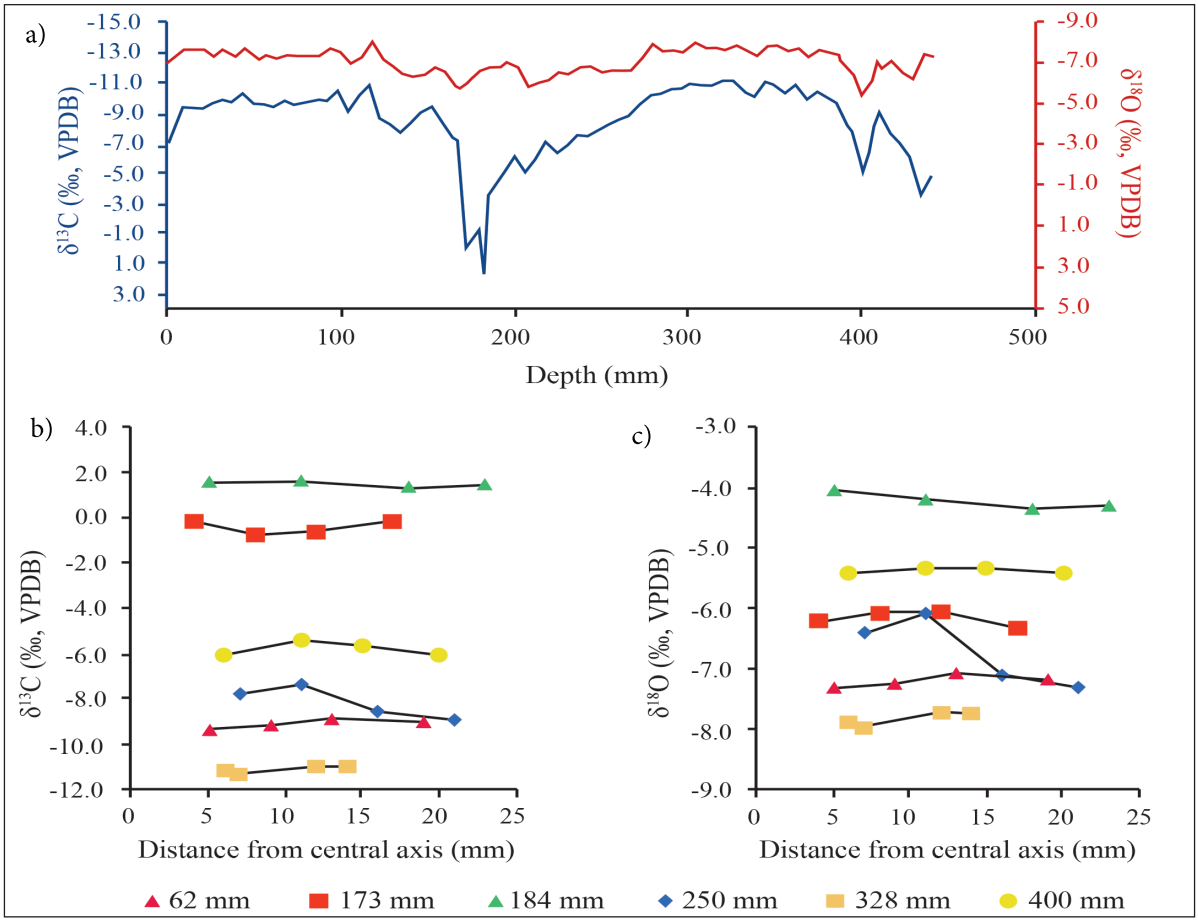

Figure 7. Hendy test for stalagmite SR04-ST3. Each sample set was drilled from the single growth layers and distances were measured from the top 400, 328, 250, 184, 173, and 62 mm.

rainfall being responsible for lower $\delta^{18}O$ values leads to more plant-respired CO_2 input into the groundwater that results in more negative $\delta^{13}C$ of speleothem carbonate (Burns et al., 2002).

In addition, an increase in the volume of precipitation causes lower $\delta^{18}O$ values and also can reduce the water/rock ratio in the interaction (i.e. dilution), leading to the decrease in the host limestone-derived ^{13}C-enriched carbon, resulting in positive correlation between stalagmite $\delta^{18}O$ and $\delta^{13}C$ (Figure 10; Li et al. 2000; Burns et al. 2002).

6.3. Implications for Indo-Australian monsoon climate

There is a robust discussion in the literature regarding whether the position and intensity of the Late Glacial Indo-Australian summer monsoon (IASM) was controlled by mainly NH high-latitude climate (Asian winter monsoon) or by SH westerlies linked to Milankovitch forcing. Some authors have argued that the strength of the IASM is largely influenced by millennial-scale climate anomalies originating in the North Atlantic (Griffith et al., 2009). Such cooling events are thought to have produced a significant reduction in the Atlantic meridional overturning circulation, which results in the strengthening of the Siberian High (or Siberian Anticyclone), responsible for southward displacement of the ITCZ toward the wetter SH (Broccoli et al., 2006).

Millennial-scale southward migration of the ITCZ is consistent with drier conditions indicated by stalagmite $\delta^{18}O$ records from the Hulu and Dongge Caves (Wang et al., 2001, 2008) in China and from northern Borneo (Gunung Buda) located just to the north of the equator (4° N, 114° E). On the other hand, records from the island of Flores (8° S, 121° E) show an anti-phased relationship with a strengthening of IASM, during Heinrich events and the YD, which is also consistent with this hypothesis (Griffith et al., 2009; Muller et al., 2012).

$\delta^{18}O$ data and the timing of growth phases in stalagmite SR04-ST3 that was collected from a site in SW Sulawesi within the intervening region of the latitudinally migrating ITCZ (Figure 2) reveal some transitional climatic features. The SR04-ST3 $\delta^{18}O$ time series for the 10.4–11.6 ka period, Borneo (Partin et al., 2007), and Tangga stalagmite $\delta^{18}O$

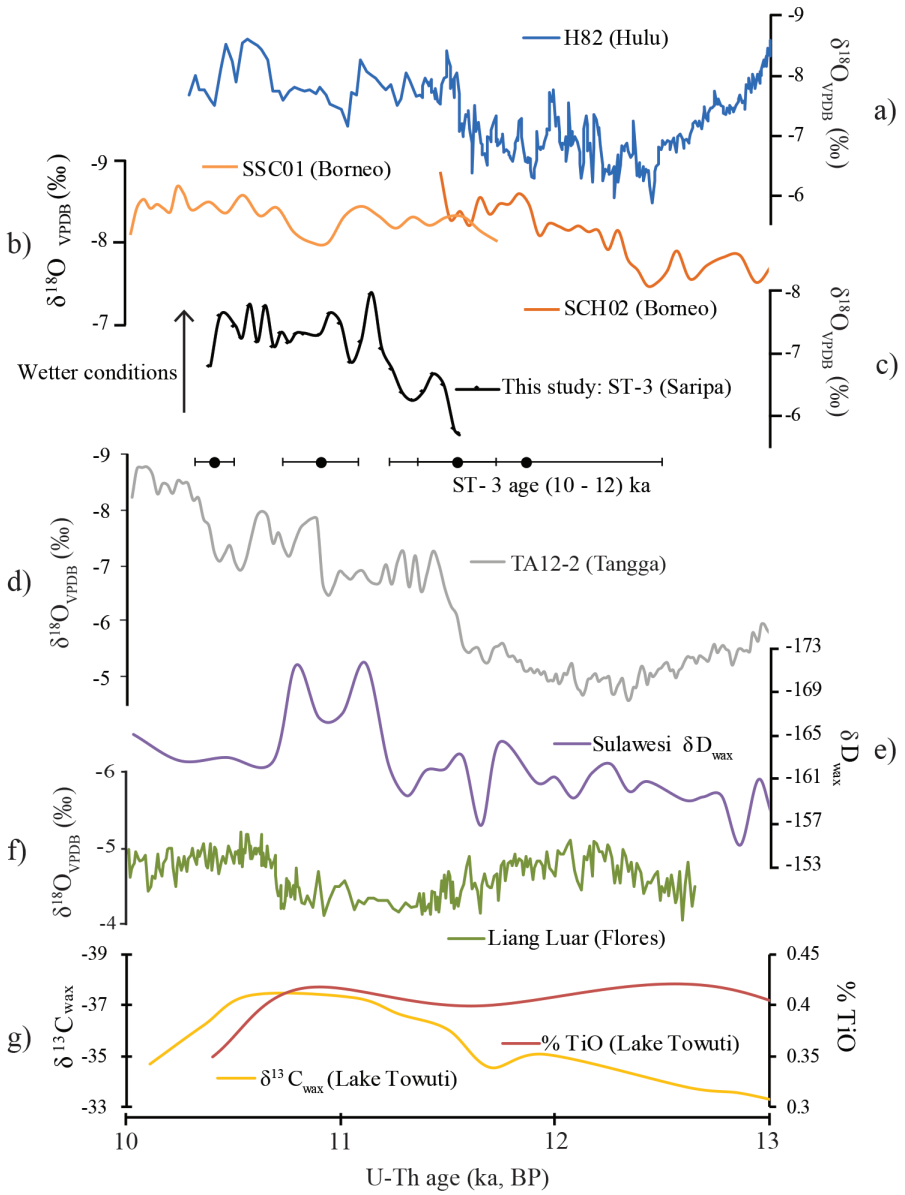

Figure 8. Comparison of the stalagmite SR04-ST3 $\delta^{18}O$ records with those of the Hulu Cave (Wang et al., 2001) (a) representing NH palaeoclimate archives and other nearby climate proxy records from the region, such as speleothems in N Borneo (b) (Partin et al., 2007) and Sumatra (d) (Wurtzel et al., 2018), marine leaf wax (from offshore Sulawesi) (Tierney et al., 2012) (e), Liang Luar, Flores (Griffiths et al., 2009; Ayliffe et al., 2013) (f), and lake records (from Lake Towuti in central Sulawesi) (Russell et al., 2014) (g) for the 13–10 ka period. This study's records are shown in (c).

records (Wurtzel et al., 2018) and leaf wax hydrogen isotope data recorded from offshore Sulawesi during the same period (Tierney et al., 2012) show similarities to that of the Hulu record and indicate wetter conditions, but display an anti-phase relationship with the Flores (Liang Luar) record (Griffith et al., 2009) (Figure 8). By contrast, the negative $\delta^{18}O$ excursion of the other major growth phase at 43.8–44.7 ka in the Saripa Cave stalagmite correlates with dry periods of the Hulu record within the respective dating errors of the two records and suggests an anti-phased relationship between the Sulawesi stalagmite and the NH Hulu record (Figure 9).

Such a bipolar seesaw relationship in rainfall patterns between the SH and NH, particularly between the Indo-Australian and East Asian summer monsoons, can most easily be attributed to the latitudinal shift of the ITCZ and SH storm tracks (Griffith et al., 2009; Ayliffe et al., 2013; Markle et al., 2017). Our results suggest that rainfall seasons

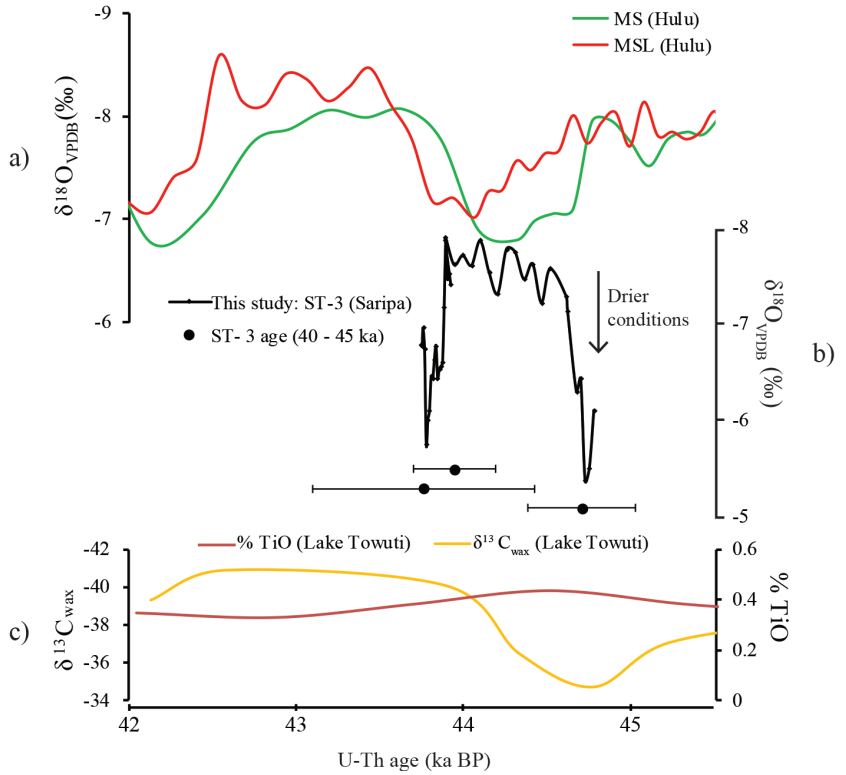

Figure 9. Saripa Cave stalagmite (SR04-ST3) $\delta^{18}O$ record compared with other paleoclimate records for the 46–42 ka period. (a) Hulu Cave records (MS and MSL speleothems (Wang et al., 2001). (b) This study. (c) Lake Towuti records (from central Sulawesi) (Russell et al., 2014).

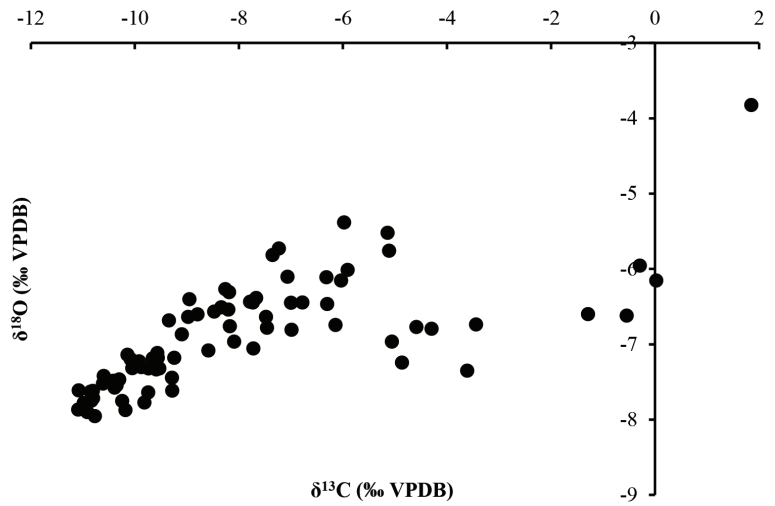

Figure 10. $\delta^{18}O$ vs. $\delta^{13}C$ correlation for the Saripa Cave stalagmite (SR04-ST3).

in Southwest Sulawesi may have changed dramatically, resulting in both in-phase and anti-phase relationships with the NH records in different times depending on the mean location of the ITCZ. Furthermore, it was argued in a model study that Antarctic-sourced meltwater bursts can change the climate globally as an additional mechanism that is likely to be associated with a pronounced ocean-atmosphere bipolar seesaw (Turney et al., 2017). Thus, it is noted that the seesaw relationship captured in this study might also be influenced by Antarctic-Southern Ocean climate dynamics.

In short, the growth phases in Saripa Cave speleothem ST-3 (Figures 3 and 6) relate to periods of abundant moisture in this part of Sulawesi. We interpret the change in speleothem calcite oxygen isotope values (Figures 8 and 9) as representing changes in the water masses themselves and actually likely to reflect changes in the isotopic composition of waters in the moisture source areas.

6.4. Isotope and trace element anomalies as evidence of transient environmental events

The growth record of SR04-ST3 is fragmented with only a few short growth phases and interrupted by long-lasting growth hiatuses (Figure 6). There are no growth hiatuses immediately below and above the optically dark layers at 184 mm (~20 ka) (Figure 3), and hence the surrounding layers are thought to represent continuous growth. The Hendy test shows that these layers formed in isotope equilibrium, suggesting that their anomalous $\delta^{18}O$ and $\delta^{13}C$ values are not due to kinetic isotope fractionation and thus must record the composition of the precipitating fluids and/or a possible climatic signal. The optically dark layer at 184 mm, together with the continuous section below and above it, formed between 22 and 20 ka (Figure 3). This interval started with a $\delta^{18}O$ of –6.7‰, which is the same value as that at 11.2 ka. However, a marked increase of $\delta^{18}O$ to a value of–3.8‰ and a sudden enrichment of more than 10‰ for $\delta^{13}C$ are evident (Figure 3). This, together with a sharp enrichment of trace element abundance at 184 mm and an immediate return to lower and more typical $\delta^{18}O$-$\delta^{13}C$ values and trace element contents at 184 mm (Figure 3), as well as the enrichments (especially in O and C isotopes) at ~403 mm, suggest the impact of short-term events. Such events may be related to episodes of transient local climate change or volcanic activities.

Speleothem-derived trace element concentrations (e.g., Sr or Sr/Ca profiles) possess important information about past hydrological changes, specifically in soil-water-rock interactions (e.g., Fairchild and Treble, 2009; Griffiths et al., 2010). Variations in rainfall amount, prior calcite precipitation, and residence time of drip waters within the cave system affect the stalagmite-forming drip water chemistry (e.g., Ünal-İmer et al., 2016a). In this study, although it is not consistent through the whole record of the Saripa Cave speleothem (SR04-ST3) and the resolutions are different, it is noted that the $\delta^{18}O$-$\delta^{13}C$ record is more negative when Sr (ppm) and Sr/Ca (ppm/ppm) values are lower and vice versa (Figure 3). This could be related to the changes in paleohumidity or in moisture balance, linking the changes in Sr and Sr/Ca values to dry-wet conditions, with relatively higher values indicative of drier conditions (e.g., Regattieri et al., 2014). It is also apparent that there is no rapid variation in Sr content or Sr/Ca ratio at optically dark layers (e.g., 22–20 ka, 184 mm), opposite of the other trace elements (Cr, Rb, Ti, Mn, and Th). Similar to the Saripa Cave record, the Bumi Cave stalagmite (BC-09-3-C) shows a decreasing trend in Sr (ppm) and Sr/Ca (ppm/ppm) values as $\delta^{18}O$ values become depleted (Figure 5), although it is not clear from the profile due to the difference in analytical resolution. Again, this might be reflecting that the Sr values and Sr/Ca ratios can be used as tracers of moisture balance, suggesting drier conditions with higher values.

6.4.1. Climate implications

It is a common phenomenon that both $\delta^{18}O$ and $\delta^{13}C$ in speleothems are interpreted to be higher (enriched) during cold/dry intervals (Wang et al., 2001; Genty et al., 2003, 2006; Rudzka et al., 2011). Particularly, the increase in $\delta^{13}C$ can be due to decreased inputs of isotopically light biogenic carbon from soil and vegetation sources during cold/dry climatic conditions. As discussed above (see the last paragraph of Section 6.2), this is explained by lower CO_2 soil production and an increased proportion of dissolved inorganic carbon through limestone dissolution (Rudzka et al., 2011). Continued cave water-host rock interaction during dry climate episodes in the Saripa Cave would result in enrichment of the seepage waters by more host rock-derived trace elements yielding the enrichment in Cr, Ti, Mn, Rb, and Th at ~20–25 ka in the ST-3 speleothem (Figure 3). However, either cold or dry climatic conditions are highly unlikely to control the main changes of the $\delta^{13}C$ record in the Saripa Cave and Bumi Cave speleothems from N Sulawesi, since this area is so wet and hence cessation of speleothem growth is unlikely, though any reduction in rainfall should diminish the growth rate. In addition, if such significant $\delta^{18}O$ and $\delta^{13}C$ increases were due to climatic changes they should also be evident in other regional climate records discussed above, as well as in the Bumi stalagmite. Therefore, an overprinting of a volcanic signal on $\delta^{18}O$ and $\delta^{13}C$ values of the dark layers is conceivable (see the discussion below).

6.4.2. Possible effect of volcanic activities

SO_2 ejected during explosive volcanic activity changes the loading level of the stratospheric sulfate aerosol that can be recorded in cave deposits (Frisia et al., 2008). S from volcanic emissions reaches the cave soil and is incorporated in the growing speleothem. Speleothems as archives of precisely dated past volcanic eruptions have been used by applying synchrotron radiation-based (SR) X-ray microfluorescence to laminated stalagmites (Frisia et al., 2005). Volcanic activities also play a key role in triggering CO_2 degassing, changing the flow regime and the chemistry of groundwater systems (Karabacak et al., 2017). During times of significant volcanic and/or tectonic activities high CO_2 production is common as a result of mantle degassing and dissolution of limestone formations (Salazar et al., 2004; Chiodini et al., 2007; Freda et al., 2011; Ünal-İmer et al., 2016b). Sufficiently high CO_2

accumulation beneath volcanoes may trigger phreatic eruptions (e.g., Dieng Volcanic Plateau, Indonesia) or earthquake swarms with the voluminous CO_2 emission and absorption into shallow groundwater (Allard et al., 1989; Giggenbach et al., 1991; Evans et al., 2002; D'Alessandro et al., 2007; Shelly et al., 2013). CO_2 enrichment can lead to increased acidification and hence undersaturation of the groundwater with respect to $CaCO_3$ resulting in the interruption of carbonate precipitation (c.f., Tuccimei et al., 2006). This is consistent with the growth hiatuses followed by precipitations of the optically dark layers in SR04-ST3 (Figures 3 and 4). As the carbonate saturation increases (a function of the cation concentration, pH, and $[CO_3^{2-}]$, the precipitation of the first carbonate layer (dark layers) will take place from a fluid that is not only enriched in CO_2 but also contains high amounts of trace elements. The latter arises from the fact that mineral solubilities in CO_2-H_2O fluids initially increase due to the decrease in the pH of the system and the formation of bicarbonate ions. This may explain the spike in trace elements evident especially at 184 mm (Figure 3). Alternatively, this layer may represent the reduced deposition and accumulation of detrital material, enriched in trace elements. Also, the reduced growth rate may have originated from reduced infiltration, i.e. longer water residence time, elevated amount of rock-derived carbon, and stronger degassing-evaporation processes, resulting in higher $\delta^{13}C$ and $\delta^{18}O$ values.

Another process that can lead to both an increase in $\delta^{13}C$ and trace element enrichment is cave ventilation. Because of drops in pCO_2 in well ventilated cave passages, CO_2 degassing from cave water is enhanced. This will result in the preferential loss of isotopically light CO_2 and hence an increase in the $\delta^{13}C$ of the remaining solutions from which the speleothem was deposited (Spötl et al., 2005). Through cave ventilation trace elements can be introduced from aerosol sources entering cave networks (Dredge et al., 2013). Aerosols are sourced mainly from local windblown sands and widespread volcanic eruptions in the region. Particle accumulation occurs as both dry deposition (in the absence of precipitation) and scavenging by atmospheric hydrometeors (wet deposition) (Mather et al., 2003). Volcanic aerosols may originate from pyroclastic material (tephra), condensation of volcanic gases, volatile elements released from the magma, and the boiling of hydrothermal fluids (Mather et al., 2003).

Elemental enrichments occur particularly at hiatuses or during periods of slow speleothem growth. Sr isotope ratios can indicate the geological source region of terrestrial dust (e.g., Frumkin and Stein, 2004; Cheng et al., 2010). Volcanic eruptions are a more likely scenario providing aerosols through cave ventilation (c.f., Dredge et al., 2013). This can also be exemplified by Badertscher et al. (2014) reporting that a stalagmite from Sofular Cave (N Turkey) shows sudden short-lived peaks in bromine, sulfur, and molybdenum, which is attributed to a Minoan volcanic eruption between 1600 and 1650 BC. Low Sr isotopic values of the Saripa Cave stalagmite (at 184 mm, ~20 ka) reflecting young volcanic sources, particularly in the intervals following the precipitation of the optically dark layer (Figure 3), are consistent with the notion of aerosols derived from volcanic sources. Therefore, we could suggest that there was possible volcanic activity at around ~22 ka. However, the Bumi stalagmite has much higher $^{87}Sr/^{86}Sr$ values (Table 5). This may be due to different cave morphologies and local circulation, which strongly influence the transport and deposition of aerosols throughout the cave network, whereby volcanic aerosols reach one cave in volume while being rare or absent in the other (e.g., Dredge et al., 2013). Alternatively, different $^{87}Sr/^{86}Sr$ values for these caves could also reflect the change in the contribution of the two $^{87}Sr/^{86}Sr$ end members, with the less radiogenic soil source derived from the weathering of volcanic rocks above the Saripa Cave and more radiogenic host-carbonate sourced Sr at the Bumi Cave.

7. Conclusions

Stalagmites from the Saripa Cave and Bumi Cave in Sulawesi, SW Indonesia, provide information about a region affected by both climate changes and sudden volcanic eruptions, within an area influenced by both SH and NH processes. The timing of growth as well as the $\delta^{18}O$ values for different growth phases in the stalagmite sample from the Saripa Cave indicates both anti-phase (43.8–44.7 ka) and in-phase (10.4–11.6, 46.4, 52.0, 76.7–77.4 ka) relationships with the NH records. Such an observation is unique in the Western Pacific tropical region, with rainfall seasons changing dramatically from NH summers to SH summers depending on the mean location of the ITCZ. The stalagmite contains several optically dark laminae, which show a sudden increase in trace element abundance and $\delta^{18}O$ and $\delta^{13}C$ values, and a drop in $^{87}Sr/^{86}Sr$. Such remarkable trace element and isotopic changes are interpreted as a record of non-climate environmental events, possibly related to volcanism. Millimeter- to submillimeter-scale geochemical investigations and precise age dating of speleothems from tectonically active regions are unique tools for reconstructing both Quaternary climate history and unexpected natural events such as abrupt changes caused by volcanic eruptions.

Acknowledgments

This study was supported by Australian Research Council (ARC) grants DP0663274 (to Mike Gagan, Wahyoe Hantoro, and JXZ) and DP077308 (to JXZ), an Australian Postgraduate Award to ESP, and the Queensland Geothermal Centre of Excellence funded by the Queensland

State Government. The project was conducted in Indonesia under Kementerian Negara Risetdan Teknologi (RISTEK) research permit number 04/TKPIPA/FRP/SM/IV/2009 (to Mike Gagan). We are particularly grateful to the Research Center for Geotechnology, Indonesian Institute of Sciences (LIPI), and staff of Bantimurung-Bulusaraung National Park for their logistical support, including the invaluable assistance of Bambang Suwargadi (LIPI) and Saiful Fajirin (B-BNP) in the field. Gavin Dunbar led the fieldwork and Jol Desmarchelier, Neil Anderson, and Dan Zwartz provided expertise in technical caving and cave conservation. We thank Yue-xing Feng for assistance with U-series dating at UQ and Heather Scott-Gagan and Joe Cali for C-O isotope measurements at the Research School of Earth Sciences, ANU. We appreciatively acknowledge Chris Jennings for his help drawing some of the figures.

References

Allard P, Dajlevie D, Delarue C. (1989). Origin of carbon dioxide emanation from the 1979 Dieng eruption, Indonesia; implications for the origin of the 1986 Nyos catastrophe. Journal of Volcanology and Geothermal Research 39: 195-206.

Ayliffe LK, Gagan MK, Zhao JX, Drysdale RN, Hellstrom JC et al. (2013). Rapid interhemispheric climate links via the Australasian monsoon during the last deglaciation. Nature Communications. doi: 101038/ncomms3908

Badertscher S, Borsato A, Frisia S, Cheng H, Edwards RL et al. (2014). Speleothems as sensitive recorders of volcanic eruptions–the Bronze Age Minoan eruption recorded in a stalagmite from Turkey. Earth and Planetary Science Letters 392: 58-66.

Broccoli AJ, Dahl KA, Stouffer RJ (2006). Response of the ITCZ to Northern Hemisphere cooling. Geophysical Research Letters 33: L01702. doi: 101029/2005GL024546

Burke WH, Denison RE, Hetherington EA, Koepnick RB, Nelson HF et al. (1982). Variation of seawater $^{87}Sr/^{86}Sr$ throughout Phanerozoic time. Geology 10: 516-519.

Burns SJ, Fleitmann D, Mudelsee M, Neff U, Matter A et al. (2002). A 780-year annually resolved record of Indian Ocean monsoon precipitation from a speleothem from South Oman. Journal of Geophysical Research—Atmospheres 107: 4434.

Cane MA, Clement AC (1999). A role for the tropical Pacific coupled ocean-atmosphere system on Milankovich and millennial timescales. Part II: Global impacts. In: Clark PU (editor). AGU Monograph: Mechanisms of Global Climate Change at Millennial Time Scales. Oxford, UK: Blackwell, pp. 363-371.

Cheng MC, You CF, Lin FJ, Chung CH, Huang KF (2010). Seasonal variation in long-range transported dust to a subtropical islet offshore northern Taiwan: chemical composition and Sr isotopic evidence in rainwater. Atmospheric Environment 44: 3386-3393.

Chiodini G, Angela F, Barberi ML, Carapezza C, Cardellini F et al. (2007). Carbon dioxide degassing at Latera caldera (Italy): evidence of geothermal reservoir and evaluation of its potential energy. Journal of Geophysical Research 112 (B12): 17.

Clark TR, Zhao JX, Roff G, Feng YX, Donec TJ et al. (2014). Discerning the timing and cause of historical mortality events in modern Porites from the Great Barrier Reef. Geochimica et Cosmochimica Acta 138: 57-80.

D'Alessandro W, Glammanco S, Bellomo S, Parello F (2007). Geochemistry and mineralogy of travertine deposits of the SW flank of Mt Etna (Italy): relationships with past volcanic and degassing activity. Journal of Volcanology and Geothermal Research 165 (1-2): 64-70.

Dansgaard W (1964). Stable isotopes in precipitation. Tellus 16: 436-468.

Dredge J, Fairchild IJ, Harrison RM, Fernandez-Cortes A, Sanchez-Moral S et al. (2013). Cave aerosols: distribution and contribution to speleothem geochemistry. Quaternary Science Reviews 63: 23-41.

Evans WC, Sorey ML, Cook AC, Kennedy BM, Shuster DL et al. (2002). Tracing and quantifying magmatic carbon discharge in cold ground waters: lessons learned from Mammoth Mountain, USA. Journal of Volcanology and Geothermal Research 114: 291-312.

Fairchild IJ, Treble, PC (2009). Trace elements in speleothems as recorders of environmental change. Quaternary Science Reviews 28 (5-6): 449-468.

Fleitmann D, Burns SJ, Neff, U, Mudelsee M, Mangini A (2004). Palaeoclimatic interpretation of high-resolution oxygen isotope profiles derived from annually laminated speleothems from southern Oman. Quaternary Science Reviews 23: 935-945.

Fleitmann D, Cheng H, Badertscher S, Edwards RL, Mudelsee M et al. (2009). Timing and climatic impact of Greenland interstadials recorded in stalagmites from northern Turkey. Geophysical Research Letters 36 (19): 1–5.

Freda C, Gaeta M, Giaccio B, Marra F, Palladino DM et al. (2011). CO_2-driven large mafic explosive eruptions: the Pozzolane Rosse case study from the Colli Albani Volcanic District (Italy). Bulletin of Volcanology 73: 241-256.

Friedman I, O'Neil JR (1977). Data of Geochemistry. US Geological Survey (USGS) Professional Paper 440-KK, KK1-12. Washington, DC, USA: USGS.

Frisia S, Borsato A, Susini J (2008). Synchrotron radiation applications to past volcanism archived in speleothems: an overview. Journal of Volcanology and Geothermal Research 177: 96-100.

Frisia S, Borsato A, Fairchild, IJ, Susini J (2005). Variations in atmospheric sulphate recorded in stalagmites by synchrotron micro-XRF and XANES analyses. Earth and Planetary Science Letters 235: 729-740.

Frumkin A, Stein M (2004). The Sahara–East Mediterranean dust and climate connection revealed by strontium and uranium isotopes in a Jerusalem speleothem. Earth and Planetary Science Letters 217: 451-464.

Genty D, Blamart D, Ghaleb B, Plagnes V, Causse CH et al. (2006). Timing and dynamics of the last deglaciation from European and North African d13C stalagmite profiles–comparison with Chinese and South Hemisphere stalagmites. Quaternary Science Reviews 25: 2118-2142.

Genty D, Blamart D, Ouahdi R, Gilmour M, Baker A et al. (2003). Precise dating of Dansgaard-Oeschger climate oscillations in western Europe from stalagmite data. Nature 421: 833-837.

Giggenbach WF, Sano Y, Schmincke HU (1991). CO_2-rich gases from lakes Nyos and Monoun, Cameroon; Laacher See, Germany; Dieng, Indonesia, and Mt. Gambier, Australia: variations on a common theme. Journal of Volcanology and Geothermal Research 45: 311-323.

Griffiths ML, Drysdale RN, Gagan MK, Frisia S, Zhao JX et al. (2010). Evidence for Holocene changes in Australian-Indonesian monsoon rainfall from stalagmite trace element and stable isotope ratios. Earth and Planetary Science Letters 292: 27-38.

Griffiths ML, Drysdale RN, Gagan MK, Zhao JX, Ayliffe LK et al. (2009). Increasing Australian-Indonesian monsoon rainfall linked to Early Holocene sea-level rise. Nature Geoscience 29: 636-639.

Guntoro A (1999). The formation of the Makassar Strait and the separation between SE Kalimantan and SW Sulawesi. Journal of Asian Earth Sciences 17: 79-98.

Hall R, Wilson MEJ (2000). Neogene sutures in eastern Indonesia. Journal of Asian Earth Sciences 18: 781-808.

Hendy CH (1971). The isotopic geochemistry of speleothems-I. The calculation of the effects of different modes of formation on the isotopic composition of speleothems and their applicability as paleoclimatic indicators. Geochimica et Cosmochimica Acta 35: 801-824.

Jamieson RA, Baldini JUL, Frappier AB, Müller W (2015). Volcanic ash fall events identified using principal component analysis of a high-resolution speleothem trace element dataset. Earth and Planetary Science Letters 426: 36-45.

Kagan EJ, Agnon A, Bar-Matthews M, Ayalon A (2005). Dating large infrequent earthquakes by damaged cave deposits. Geology 33: 261-264.

Karabacak V, Uysal IT, Ünal-İmer E, Mutlu H, Zhao JX (2017). U-Th evidence from carbonate veins for episodic crustal deformation of Central Anatolian Volcanic Province. Quaternary Science Reviews 177: 158-172.

Lawrence MG, Kamber BS (2006). The behaviour of the rare earth elements during estuarine mixing-revisited. Marine Chemistry 100: 147-161.

Leterrier J, Yuwono YS, Soeria-Atmadja R, Maury RC (1990). Potassic volcanism in Central Java and South Sulawesi, Indonesia. Journal of Southeast Asian Earth Sciences 4: 171-187.

Li B, Yuan D, Qin J, Lin Y, Zhang M (2000). Oxygen and carbon isotopic characteristics of rainwater, drip water and present speleothems in a cave in Guilin area, and their environmental meanings. Science in China Series D 43: 277-285.

Ludwig KR (2012). User's Manual for Isoplot/Ex Version 3750: A Geochronological Toolkit for Microsoft Excel. Berkeley, CA, USA: Berkeley Geochronology Center.

Markle BR, Steig EJ, Buizert C, Schoenemann SW, Bitz CM et al. (2017). Global atmospheric teleconnections during Dansgaard-Oeschger events. Nature Geoscience 10: 36-40.

Mather TA, Pyle DM, Oppenheimer C (2003). Tropospheric volcanic aerosol. In: Volcanism and the Earth's Atmosphere. Washington, DC, USA; American Geophysical Union, pp. 189-212.

Mattey D, Lowry D, Duffet J, Fisher R, Hodge E et al. (2008). A 53 year seasonally resolved oxygen and carbon isotope record from a modem Gibraltar speleothem: reconstructed drip water and relationship to local precipitation. Earth and Planetary Science Letters 269: 80-95.

Muller J, McManus JF, Oppo D, Francois R, Brown-Ledger S (2012). Strengthening of the North-East Monsoon over the Flores Sea, Indonesia, at the time of Heinrich Event 1. Geology 40: 635-638.

Partin JW, Cobb KM, Adkins JF, Clark B, Fernandez DP (2007). Millennial-scale trends in west Pacific warm pool hydrology since the Last Glacial Maxim**.** Nature 449: 452-455.

Philander SGH (1983). El Nino Southern Oscillation phenomena. Nature 302: 295-301.

Quade J, Cerling TE, Bowman JR (1989). Systematic variations in the carbon and oxygen isotopic composition of pedogenic carbonate along elevation transects in the Southern Great-Basin, United-States. Geological Society of America Bulletin 101: 464-475.

Regattieri E, Zanchetta G, Drysdale RN, Isola I, Hellstrom JC et al. (2014). Late glacial to Holocene trace element record (Ba, Mg, Sr) from Corchia Cave (Apuan Alps, central Italy): paleoenvironmental implications. Journal of Quaternary Science 29 (4): 381-392.

Russell JM, Vogel H, Konecky BL, Bijaksana S, Huang Y et al. (2014). Glacial forcing of central Indonesian hydroclimate since 60,000 y BP. Proceedings of the National Academy of Science of the USA 111 (14): 5100-5105.

Rudzka D, McDermott F, Baldini LM, Fleitmann D, Moreno A et al. (2011). The coupled δ13C-radiocarbon systematics of three Late Glacial/early Holocene speleothems; insights into soil and cave processes at climatic transitions. Geochimica et Cosmochimica Acta 75: 4321-4339.

Salazar JML, Hernandez PA, Perez NM, Olmos R, Barahona F et al. (2004). Spatial and temporal variations of diffuse CO_2 degassing at Santa Ana-Izalco-Coatepeque volcanic complex, El Salvador, Central America. In: Rose WI, Bommer JJ, López Dina L, Carr MJ, Major JJ (editors). Natural Hazards in El Salvador. Boulder, CO, USA: Geological Society of America Special Papers, pp. 135-146.

Scroxton N, Gagan MK, Dunbar GB, Ayliffe LA, Hantoro WS et al. (2016). Natural attrition and growth frequency variations of stalagmites in southwest Sulawesi over the past 530,000 years. Palaeogeography, Palaeoclimatology, Palaeoecology 441: 823-833.

Shelly DR, Hill DP, Massin F, Farrell J, Smith RB et al. (2013). A fluid-driven earthquake swarm on the margin of the Yellowstone caldera. Journal of Geophysical Research 118: 4872-4886.

Siklosy Z, Demeny A, Vennemann TW, Pilet S, Kramers J et al. (2009). Bronze Age volcanic event recorded in stalagmites by combined isotope and trace element studies. Rapid Communications in Mass Spectrometry 23: 801-808.

Spötl C, Fairchild I, Tooth AF (2005). Cave air control on dripwater geochemistry, Obir Caves (Austria): implications for speleothem deposition in dynamically ventilated caves. Geochimica et Cosmochimica Acta 69 (10): 2451-2468.

St Pierre E, Zhao JX, Dunbar GB, Gagan MK (2007). Speleothem record of palaeoenvironmental change in southern Sulawesi, Indonesia during the last glacial to Holocene transition. Quaternary International 167-168: 395.

Stothers RB (1984). The great Tambora eruption in 1815 and its aftermath. Science 224: 1191-1198. doi: 10.1126/science.224.4654.1191

Tierney JE, Oppo DW, Le Grande AN, Huang Y, Rosenthal Y et al. (2012). The influence of Indian Ocean atmospheric circulation on warm pool hydroclimate during the Holocene epoch. Journal of Geophysical Research 117: D19108. doi: 101029/2012jd018060

Tuccimei P, Giordano G, Tedeschi M (2006). CO_2 release variations during the last 2000 years at the Colli Albani volcano (Roma, Italy) from speleothems studies. Earth and Planetary Science Letters 243: 449-462.

Turney CSM, Jones RT, Phipps SJ, Thomas Z, Hogg A et al. (2017). Rapid global ocean-atmosphere response to Southern Ocean freshening during the last glacial. Nature Communications 8: 520. doi: 101038/s41467-017-00577-6

Ünal-İmer E, Shulmeister J, Uysal IT, Zhao JX, Feng YX (2016a). High-resolution trace element and stable isotope profiles of late Pleistocene to Holocene speleothems from Dim Cave, SW Turkey. Palaeogeography, Palaeoclimatology, Palaeoecology 452: 68-79.

Ünal-İmer E, Uysal IT, Zhao JX, Işık V, Shulmeister J et al. (2016b). CO_2 outburst events in relation to seismicity: Constraints from micro-scale geochronology and geochemistry of Late Quaternary vein carbonates, SW Turkey. Geochimica et Cosmochimica Acta 187: 21-40.

Uysal IT, Feng Y, Zhao JX, Altunel E, Weatherley D et al. (2007). U-series dating and geochemical tracing of Late Quaternary travertine in co-seismic fissures. Earth and Planetary Science Letters 257: 450-462.

Uysal IT, Feng Y, Zhao JX, Işik V, Nuriel P et al. (2009). Hydrothermal CO_2 degassing in seismically active zones during the late Quaternary. Chemical Geology 265: 442-454.

van Leeuwen T (1981). The geology of Southwest Sulawesi with special reference to the Biru area. Geology and Tectonics of Eastern Indonesia, Geological Research and Development Centre Special Publications 2: 277-304.

Visser K, Thunell R, Stott L (2003). Magnitude and timing of temperature change in the Indo-Pacific warm pool during deglaciation. Nature 421 (6919): 152-155.

Wang YJ, Cheng H, Edwards RL, An ZS, Wu JY et al. (2001). A high-resolution absolute-dated Late Pleistocene monsoon record from Hulu Cave, China. Science 294: 2345-2348.

Wang YJ, Cheng H, Edwards RL, Kong XG, Shao XH et al. (2008). Millennial- and orbital-scale changes in the East Asian monsoon over the past 224,000 years. Nature 451: 1090-1093.

Wilson MEJ, Bosence DWJ, Limbong A (2000). Tertiary syntectonic carbonate platform development in Indonesia. Sedimentology 47: 395-419.

Wurtzel JB, Abram NJ, Lewis SC, Bajo P, Hellstrom JC et al. (2018). Tropical Indo-Pacific hydroclimate response to North Atlantic forcing during the last deglaciation as recorded by a speleothem from Sumatra, Indonesia. Earth and Planetary Science Letters 492: 264-278.

Wynn PM, Fairchild IJ, Baker A, Baldini JUL, McDermott F et al. (2008). Isotopic archives of sulphate in speleothems. Geochimica et Cosmochimica Acta 72 (10): 2465-2477.

Zhao JX, Hu K, Collerson KD, Xu HK (2001). Thermal ionization mass spectrometry U-series dating of a hominid site near Nanjing, China. Geology 29: 27-30.

Zielinski GA, Mayewski PA, Meeker LD, Gronvold K, Germani MS et al. (1997). Volcanic aerosol records and tephrochronology of the Summit, Greenland, ice cores. Journal of Geophysical Research 102 (C12): 26625-26640.

Zielinski GA, Mayewski PA, Meeker LD, Whitlow S, Twickler MS et al. (1994). Record of explosive volcanism since 7000 BC from GISP 2 Greenland ice core and implications for the volcano climate system. Science 264: 948-952.